1
Basics of Metal Matrix Composites

Karl Ulrich Kainer

1.1
Introduction

Metal composite materials have found application in many areas of daily life for quite some time. Often it is not realized that the application makes use of composite materials. These materials are produced *in situ* from the conventional production and processing of metals. Here, the Dalmatian sword with its meander structure, which results from welding two types of steel by repeated forging, can be mentioned. Materials like cast iron with graphite or steel with a high carbide content, as well as tungsten carbides, consisting of carbides and metallic binders, also belong to this group of composite materials. For many researchers the term metal matrix composites is often equated with the term light metal matrix composites (MMCs). Substantial progress in the development of light metal matrix composites has been achieved in recent decades, so that they could be introduced into the most important applications. In traffic engineering, especially in the automotive industry, MMCs have been used commercially in fiber reinforced pistons and aluminum crank cases with strengthened cylinder surfaces as well as particle-strengthened brake disks.

These innovative materials open up unlimited possibilities for modern material science and development; the characteristics of MMCs can be designed into the material, custom-made, dependent on the application. From this potential, metal matrix composites fulfill all the desired conceptions of the designer. This material group becomes interesting for use as constructional and functional materials, if the property profile of conventional materials either does not reach the increased standards of specific demands, or is the solution of the problem. However, the technology of MMCs is in competition with other modern material technologies, for example powder metallurgy. The advantages of the composite materials are only realized when there is a reasonable cost – performance relationship in the component production. The use of a composite material is obligatory if a special property profile can only be achieved by application of these materials.

The possibility of combining various material systems (metal – ceramic – nonmetal) gives the opportunity for unlimited variation. The properties of these new

Metal Matrix Composites. Custom-made Materials for Automotive and Aerospace Engineering.
Edited by Karl U. Kainer.

ISBN: 3-527-31360-5

materials are basically determined by the properties of their single components. Figure 1.1 shows the allocation of the composite materials into groups of various types of materials.

The reinforcement of metals can have many different objectives. The reinforcement of light metals opens up the possibility of application of these materials in areas where weight reduction has first priority. The precondition here is the improvement of the component properties. The development objectives for light metal composite materials are:

- Increase in yield strength and tensile strength at room temperature and above while maintaining the minimum ductility or rather toughness,
- Increase in creep resistance at higher temperatures compared to that of conventional alloys,
- Increase in fatigue strength, especially at higher temperatures,
- Improvement of thermal shock resistance,
- Improvement of corrosion resistance,
- Increase in Young's modulus,
- Reduction of thermal elongation.

To summarize, an improvement in the weight specific properties can result, offering the possibilities of extending the application area, substitution of common materials and optimisation of component properties. With functional materials there is another objective, the precondition of maintaining the appropriate function of the material. Objectives are for example:

- Increase in strength of conducting materials while maintaining the high conductivity,
- Improvement in low temperature creep resistance (reactionless materials),
- Improvement of burnout behavior (switching contact),
- Improvement of wear behavior (sliding contact),
- Increase in operating time of spot welding electrodes by reduction of burn outs,
- Production of layer composite materials for electronic components,
- Production of ductile composite superconductors,
- Production of magnetic materials with special properties.

For other applications different development objectives are given, which differ from those mentioned before. For example, in medical technology, mechanical properties, like extreme corrosion resistance and low degradation as well as biocompatibility are expected.

Although increasing development activities have led to system solutions using metal composite materials, the use of especially innovative systems, particularly in the area of light metals, has not been realised. The reason for this is insufficient process stability and reliability, combined with production and processing problems and inadequate economic efficiency. Application areas, like traffic engineering, are very cost orientated and conservative and the industry is not willing to pay additional costs for the use of such materials. For all these reasons metal matrix composites are only at the beginning of the evolution curve of modern materials, see Fig. 1.2.

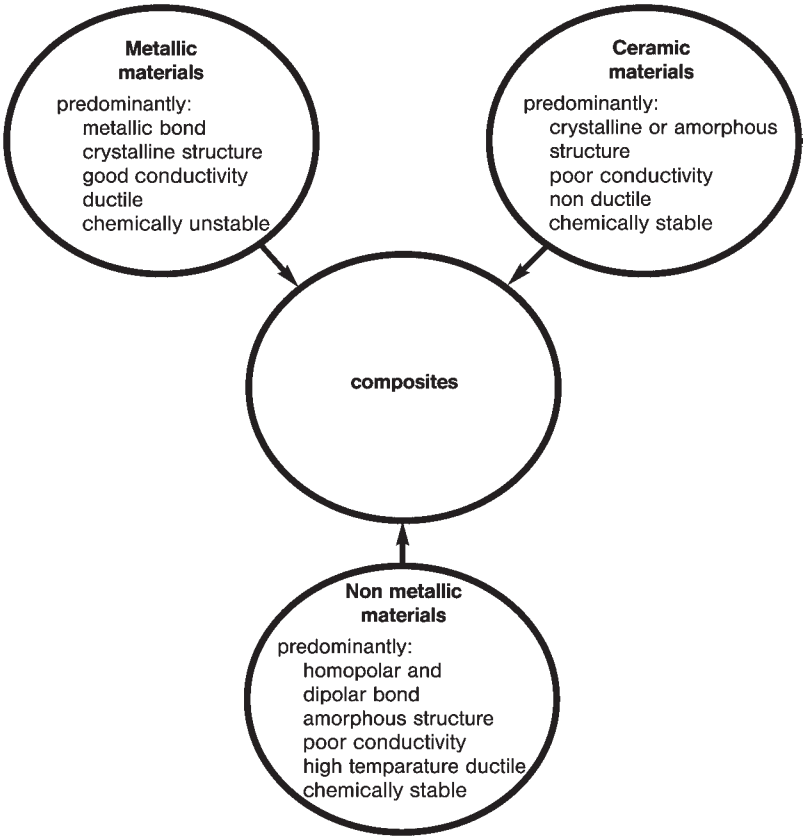

Fig. 1.1 Classification of the composite materials within the group of materials [1].

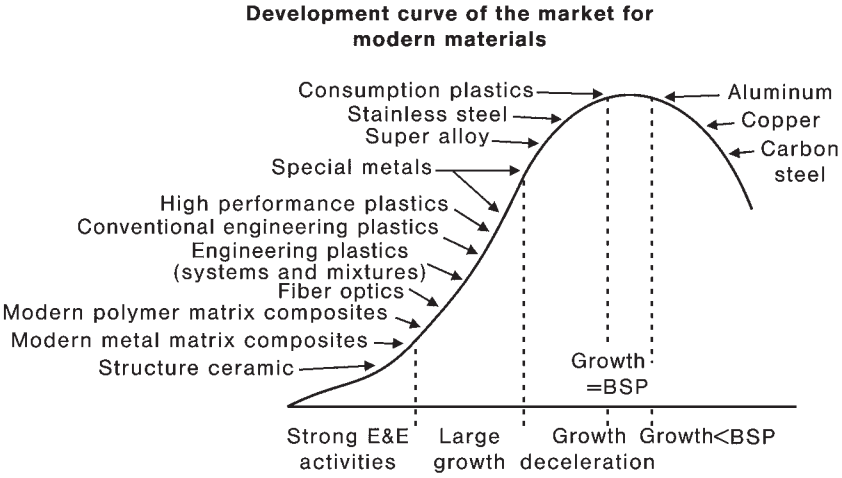

Fig. 1.2 Development curve of the market for modern materials [2].

Metal matrix composites can be classified in various ways. One classification is the consideration of type and contribution of reinforcement components in particle-, layer-, fiber- and penetration composite materials (see Fig. 1.3). Fiber composite materials can be further classified into continuous fiber composite materials (multi- and monofilament) and short fibers or, rather, whisker composite materials, see Fig. 1.4.

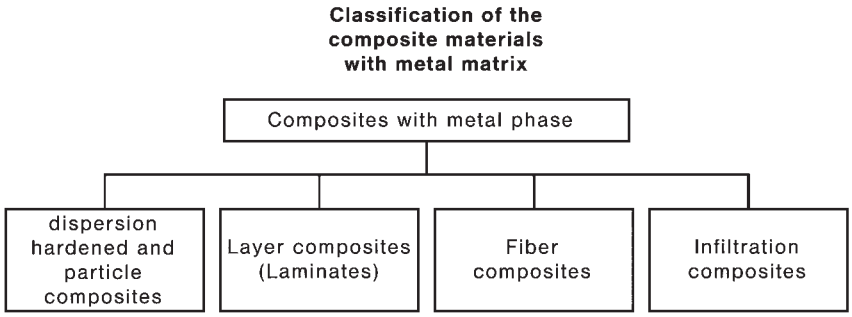

Fig. 1.3 Classification of composite materials with metal matrixes.

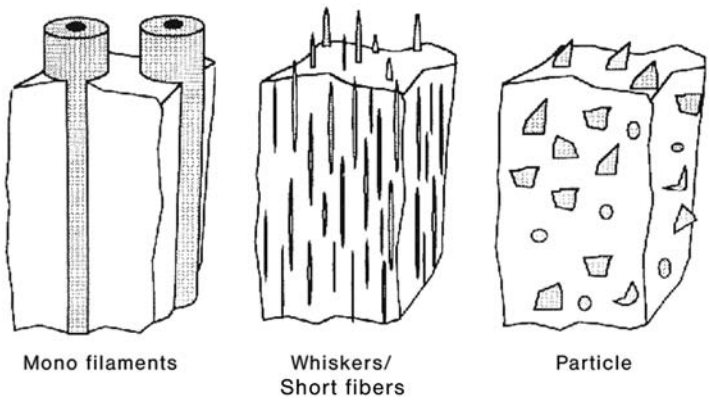

Fig. 1.4 Schematic presentation of three shapes of metal matrix composite materials [3].

1.2 Combination of Materials for Light Metal Matrix Composites

1.2.1 Reinforcements

Reinforcements for metal matrix composites have a manifold demand profile, which is determined by production and processing and by the matrix system of the composite material. The following demands are generally applicable [4]:

- low density,
- mechanical compatibility (a thermal expansion coefficient which is low but adapted to the matrix),
- chemical compatibility,
- thermal stability,
- high Young's modulus,
- high compression and tensile strength,
- good processability,
- economic efficiency.

These demands can be achieved only by using non-metal inorganic reinforcement components. For metal reinforcement ceramic particles or, rather, fibers or carbon fibers are often used. Due to the high density and the affinity to reaction with the matrix alloy the use of metallic fiber usual fails. Which components are finally used, depends on the selected matrix and on the demand profile of the intended application. In Refs. [4, 5] information about available particles, short fibers, whiskers and continuous fibers for the reinforcement of metals is given, including data of manufacturing, processing and properties. Representative examples are shown in Table 1.1. The production, processing and type of application of various reinforcements depends on the production technique for the composite materials, see Refs. [3, 7]. A combined application of various reinforcements is also possible (hybrid technique) [3, 8].

Every reinforcement has a typical profile, which is significant for the effect within the composite material and the resulting profile. Table 1.2 gives an overview of possible property profiles of various material groups. Figure 1.5 shows the specific strength and specific Young's modulus of quasi-isotropic fiber composite materials with various matrixes in comparison to monolithic metals. The group of discontinuous reinforced metals offers the best conditions for reaching development targets; the applied production technologies and reinforcement components, like short fibers, particle and whiskers, are cost effective and the production of units in large item numbers is possible. The relatively high isotropy of the properties in comparison to the long-fiber continuous reinforced light metals and the possibility

Tab. 1.1 Properties of typical discontinuous reinforcements for aluminium and magnesium reinforcements [6].

Reinforcement	*Saffil (Al_2O_3)*	*SiC particle*	*Al_2O_3 particle*
crystal structure	δ-Al_2O_3	hexagonal	hexagonal
density (g cm^{-3})	3.3	3.2	3.9
average diameter (µm)	3.0	variable	variable
length (µm)	ca. 150	–	–
Mohs hardness	7.0	9.7	9.0
strength (MPa)	2000	–	–
Young's Modulus (GPa)	300	200–300	380

Tab. 1.2 Property potential of different metal matrix composites, after [2].

MMC type	*Properties Strength*	*Young's modulus*	*High temperature properties*	*Wear*	*Expansion coefficient*	*Costs*
mineral wool: MMC	*	*	**	**	*	medium
discontinuous reinforced MMC	**	**	*	***	**	low
long fiber reinforced MMC: C fibers	**	**	**	*	***	high
other fibers	***	***	***	*	**	high

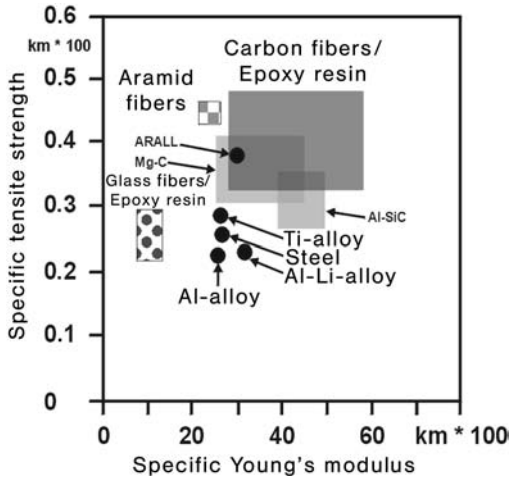

Fig. 1.5 Specific tensile strength and specific Young's modulus of different quasi-isotropic fiber composite materials in comparison to some metal alloys, after [2].

of processing of composites by forming and cutting production engineering are further advantages.

1.2.2 Matrix Alloy Systems

The selection of suitable matrix alloys is mainly determined by the intended application of the composite material. With the development of light metal composite materials that are mostly easy to process, conventional light metal alloys are applied as matrix materials. In the area of powder metallurgy special alloys can be applied due to the advantage of fast solidification during the powder production. Those systems are free from segregation problems that arise in conventional solidification. Also the application of systems with oversaturated or metastable structures is possible. Examples for matrix configurations are given in Refs. [7, 9–15]:

- conventional cast alloys
  - G-AlSi12CuMgNi
  - G-AlSi9Mg
  - G-AlSi7 (A356)
  - AZ91
  - AE42
- conventional wrought alloys
  - AlMgSiCu (6061)
  - AlCuSiMn (2014)
  - AlZnMgCu1.5 (7075)
  - TiAl6V4
- special alloys
  - Al–Cu–Mg–Ni–Fe-alloy (2618)
  - Al–Cu–Mg–Li-alloy (8090)
  - AZ91Ca

For functional materials non-alloyed or low-alloyed non-ferrous or noble metals are generally used. The reason for this is the demand for the retention of the high conductivity or ductility. A dispersion hardening to reach the required mechanical characteristics at room or higher temperatures is then an optimal solution.

1.2.3 Production and Processing of Metal Matrix Composites

Metal matrix composite materials can be produced by many different techniques. The focus of the selection of suitable process engineering is the desired kind, quantity and distribution of the reinforcement components (particles and fibers), the matrix alloy and the application. By altering the manufacturing method, the processing and the finishing, as well as by the form of the reinforcement components it is possible to obtain different characteristic profiles, although the same composition and amounts of the components are involved. The production of a suitable precursor material, the processing to a construction unit or a semi-finished material (profile) and the finishing treatment must be separated. For cost effective reasons prototypes, with dimensions close to the final product, and reforming procedures are used, which can minimize the mechanical finishing of the construction units.

In general the following product engineering types are possible:

- Melting metallurgical processes
  - infiltration of short fiber-, particle- or hybrid preforms by squeeze casting, vacuum infiltration or pressure infiltration [7, 13–15]
  - reaction infiltration of fiber- or particle preforms [16, 17]
  - processing of precursor material by stirring the particles in metallic melts, followed by sand casting, permanent mold casting or high pressure die casting [9, 10]

- Powder metallurgical processes
  - pressing and sintering and/or forging of powder mixtures and composite powders
  - extrusion or forging of metal-powder particle mixtures [11, 12]
  - extrusion or forging of spraying compatible precursor materials [7, 18, 19]
- Hot isostatic pressing of powder mixtures and fiber clutches
- Further processing of precursor material from the melting metallurgy by thixocasting or -forming, extrusion [20], forging, cold massive forming or super plastic forming
- Joining and welding of semi-manufactured products
- Finishing by machining techniques [21]
- Combined deformation of metal wires (group superconductors).

Melting metallurgy for the production of MMCs is at present of greater technical importance than powder metallurgy. It is more economical and has the advantage of being able to use well proven casting processes for the production of MMCs. Figure 1.6 shows schematically the possible methods of melting metallurgical production. For melting metallurgical processing of composite materials three procedures are mainly used [15]:

- compo-casting or melt stirring
- gas pressure infiltration
- squeeze casting or pressure casting.

Both the terms compo-casting and melt stirring are used for stirring particles into a light alloy melt. Figure 1.7 shows the schematic operational sequence of this procedure. The particles are often tend to form agglomerates, which can be only dissolved by intense stirring. However, here gas access into the melt must be absolutely avoided, since this could lead to unwanted porosities or reactions. Careful attention must be paid to the dispersion of the reinforcement components, so that the reactivity of the components used is coordinated with the temperature of the melt and the duration of stirring, since reactions with the melt can lead to the dissolution of the reinforcement components. Because of the lower surface to volume ratio of spherical particles, reactivity is usually less critical with stirred particle reinforcement than with fibers. The melt can be cast directly or processed with alternative procedures such as squeeze casting or thixocasting. Melt stirring is used by the Duralcan Company for the production of particle-strengthened aluminum alloys [9, 10]. At the Lanxide Company a similar process is used, with additional reactions between the reinforcement components and the molten matrix being purposefully promoted to obtain a qualitatively high-grade composite material [16]. In the reaction procedures of the Lanxide Company it may be desirable that the reinforcement component reacts completely with the melt to form the component *in situ*, which then transfers the actual reinforcement effect to the second phase in the MMC.

In gas pressure infiltration the melt infiltrates the preform with a gas applied from the outside. A gas that is inert with respect to the matrix is used. The melting

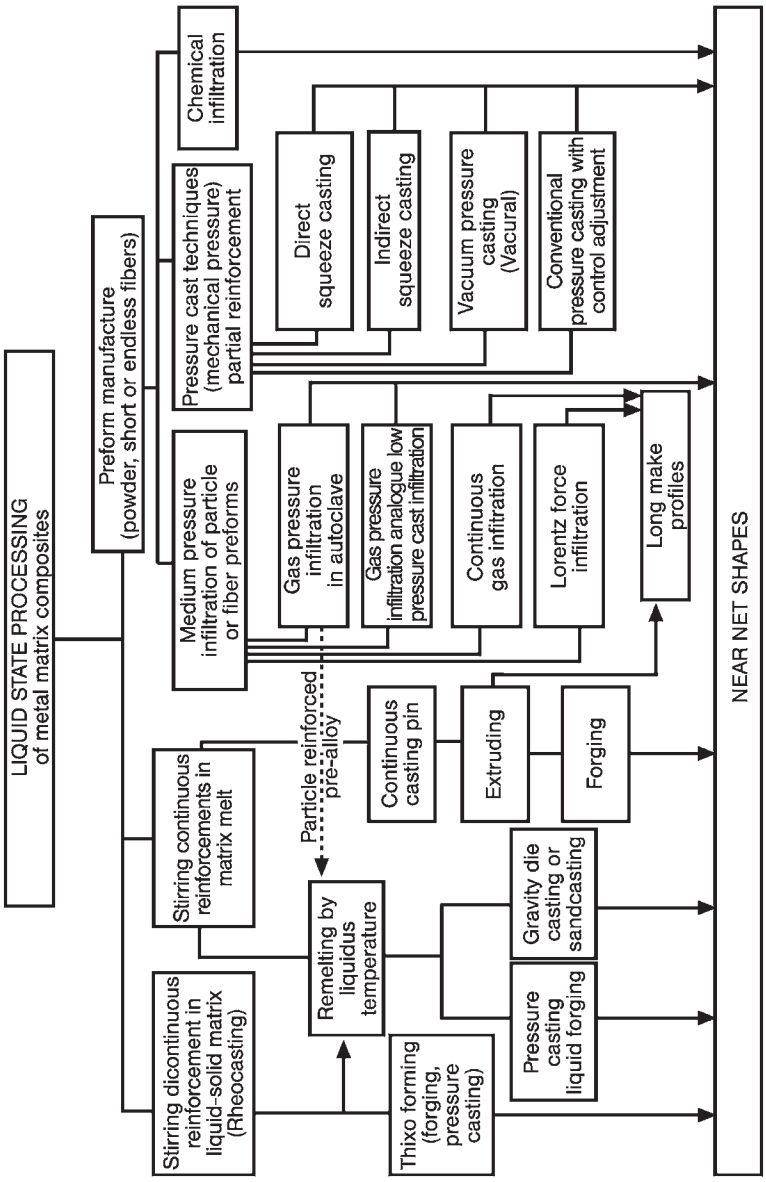

Fig. 1.6 Melting metallurgy of MMCs.

of the matrix and the infiltration take place in a suitable pressure vessel. There are two procedure variants of gas pressure infiltration: in the first variant the warmed up preform is dipped into the melt and then the gas pressure is applied to the surface of the melt, leading to infiltration. The infiltration pressure can thereby be coordinated with the wettability of the preforms, which depends, among other things, on the volume percentage of the reinforcement. The second variant of the

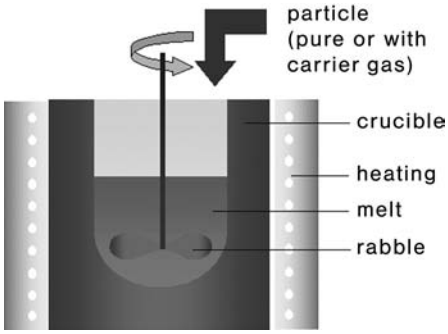

Fig. 1.7 Schematic operational sequence during melt stirring.

gas pressure infiltration procedure reverses the order: the molten bath is pressed to the preform by the applied gas pressure using a standpipe and thereupon infiltrates the bath (see Fig. 1.8). The advantage of this procedure is that there is no development of pores when completely dense parts are present. Since the reaction time is relatively short with these procedures, more reactive materials can be used than e.g. with the compo-casting. In gas pressure infiltration the response times are clearly longer than in squeeze casting, so that the materials must be carefully selected and coordinated, in order to be able to produce the appropriate composite material for the appropriate requirements.

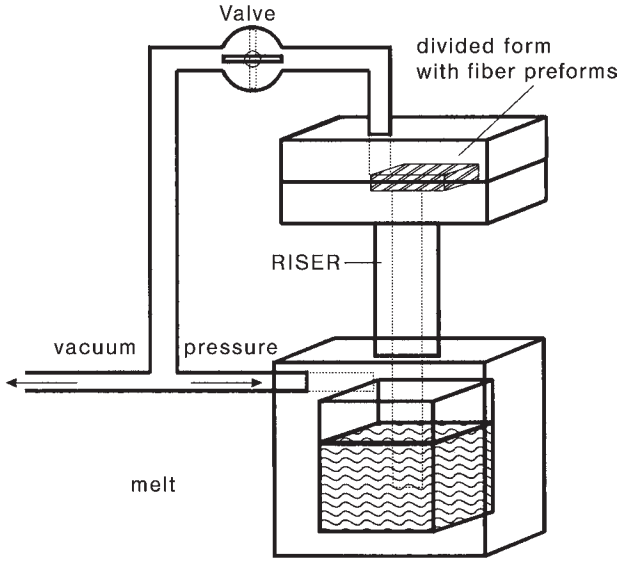

Fig. 1.8 Gas pressure infiltration technique.

Squeeze casting or pressure casting are the most common manufacturing variants for MMCs. After a slow mold filling the melt solidifies under very high pressure, which leads to a fine-grained structure. In comparison with die-casted parts the squeeze-casted parts do not contain gas inclusions, which permits thermal treatment of the produced parts. One can differentiate between direct and indirect squeeze casting (Fig. 1.9). With direct squeeze casting the pressure for the infiltration of the prefabricated preforms is applied directly to the melt. The die is thereby part of the mold, which simplifies the structure of the tools substantially. However, with the direct procedure there is a disadvantage in that the volume of the melt must be determined exactly, since no gate is present and thus the quantity of the melt determines the size of the cast construction unit. A further disadvantage is the appearance of oxidation products, formed in the cast part during dosage. In contrast, in indirect squeeze casting, where the melt is pressed into the form via a gate system, the residues will remain in this gate. The flow rate of the melt through a gate is, due to its larger diameter, substantially less than with die casting, which results in a less turbulent mold filling and gas admission to the melt by turbulences is avoided.

Both pressure casting processes make the production of composite materials possible, as prefabricated fiber or particle preforms are infiltrated with melt and solidify under pressure. A two-stage process is often used. In the first stage the melt is pressed into the form at low pressure and then at high pressure for the solidification phase. This prevents damage to the preform by too fast infiltration. The squeeze casting permits the use of relatively reactive materials, since the duration of the infiltration and thus the response time, are relatively short. A further advantage is the possibility to manufacture difficultly shaped construction units and to provide partial reinforcement, to strengthen those areas which are exposed to a higher stress during service.

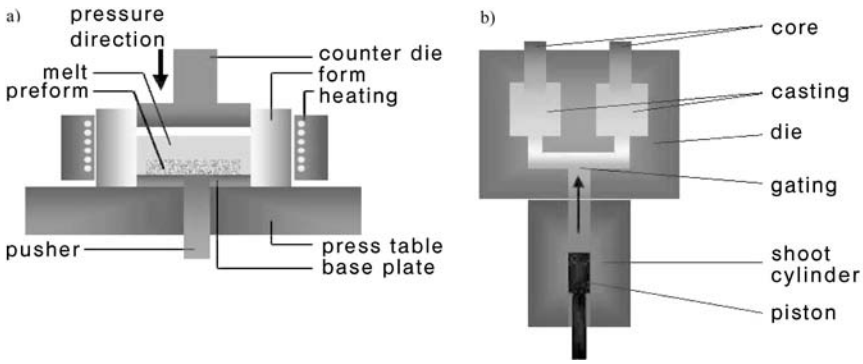

Fig. 1.9 Direct and indirect squeeze casting.

1.3 Mechanism of Reinforcement

The characteristics of metal matrix composite materials are determined by their microstructure and internal interfaces, which are affected by their production and thermal mechanical prehistory. The microstructure covers the structure of the matrix and the reinforced phase. The chemical composition, grain and/or sub-grain size, texture, precipitation behavior and lattice defects are of importance to the matrix. The second phase is characterised by its volume percentage, its kind, size, distribution and orientation. Local varying internal tension due to the different thermal expansion behavior of the two phases is an additional influencing factor.

With knowledge of the characteristics of the components, the volume percentages, the distribution and orientation it might be possible to estimate the characteristics of metallic composite materials. The approximations usually proceed from ideal conditions, i.e. optimal boundary surface formation, ideal distribution (very small number of contacts of the reinforcements among themselves) and no influence of the component on the matrix (comparable structures and precipitation behavior). However, in reality a strong interaction arises between the components involved, so that these models can only indicate the potential of a material. The different micro-, macro- and meso-scaled models proceed from different conditions and are differently developed. A representation of these models can be seen in Refs. [3, 23]. In the following, simple models are described, which facilitate our understanding of the effect of the individual components of the composite materials and their form and distribution on the characteristics of the composite.

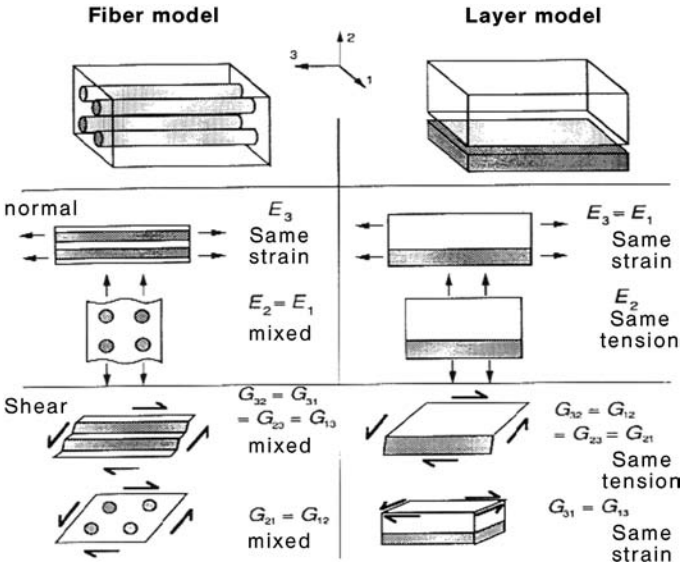

Fig. 1.10 Schematic presentation of elastic constants in composite materials.

Simply, we can consider a fiber and/or a plate model. Depending on the load direction, different elastic constants in the metallic composite material can result. Figure 1.10 illustrates the two different models and shows the resulting *E* and *G*-moduli as a function of the load type. On the basis of these simple considerations an estimate can be made of the attainable strength of the fiber reinforced composite material for the different forms of the fibers.

1.3.1
Long Fiber Reinforcement

For the optimal case of a single orientation in the direction of the stress, no fiber contact and optimal interface formation (Fig. 1.11), it is possible to use the linear mixture rule to calculate the strength of an ideal long fiber reinforced composite material with stress in the fiber orientation [23]:

$$\sigma_C = \Phi_F \cdot \sigma_F + (1 - \Phi_F) \cdot \sigma^*_M \tag{1}$$

where σ_C is the strength of the composite, Φ_F the fiber volume content, σ_F the fiber tensile strength and σ^*_M the matrix yield strength. From this basic correlation the critical fiber content $\Phi_{F,crit}$, which must be exceeded to reach an effective strengthening effect, can be determined. This specific value is important for the development of long fiber composites:

Limit of reinforcement:

$$\sigma_M = \Phi_{F,crit} \cdot \sigma_F + (1 - \Phi_{F,crit}) \cdot \sigma^*_M \tag{2}$$

Critical fiber content:

$$\Phi_{F,crit} = \frac{\sigma_M - \sigma^*_M}{\sigma_F - \sigma_M} \tag{3}$$

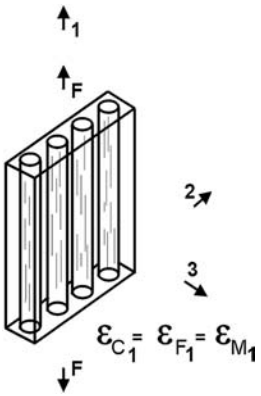

Fig. 1.11 Load of a unidirectional fiber composite layer with a force *F* in the fiber direction.

Approximation of high fiber strength:

$$\Phi_{F,crit} = \frac{\sigma_M - \sigma^*_M}{\sigma_F} \tag{4}$$

Figure 1.12 shows the dependence of the tensile strength of unidirectional fiber composite materials on the fiber content. The basis is the use of a low strength ductile matrix and of high-strength fibers with high Young's modulus. For different matrix fiber combinations different behavior of the materials results. In Fig. 1.13

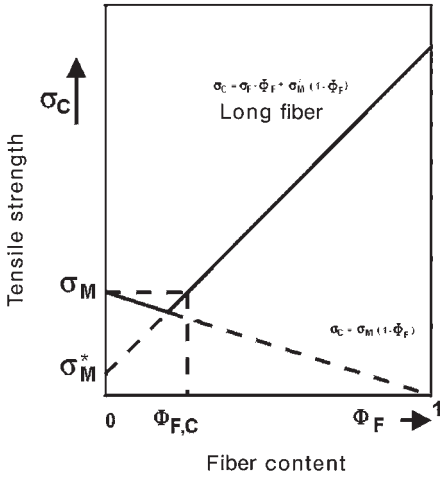

Fig. 1.12 Linear mixture rule for tensile strength of unidirectional fiber composite materials with a ductile matrix and high strength fibers [23].

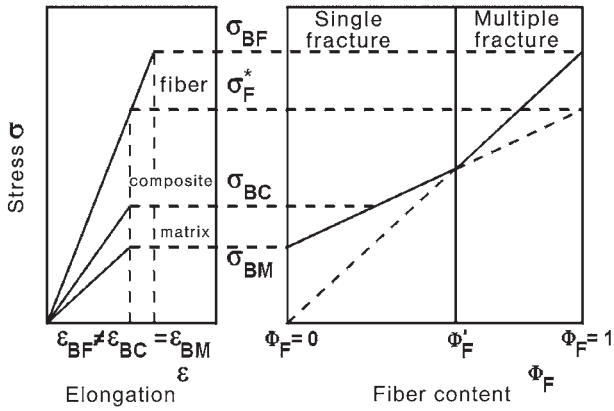

Fig. 1.13 Stress–strain behavior of a fiber composite material with a ductile matrix, in which elongation at fracture is higher than that of the fibers (σ_{BF}=tensile strength of the fiber, σ^*_F=effective fiber strength at the fracture of the composite material, σ_{BC}=strength of composite material, σ_{BM}=matrix strength, ε_{BF}= elongation at fracture of the fiber, ε_{BM}=elongation at fracture of the matrix, ε_{BC}= elongation at fracture of the composite material) [24].

the stress–strain behavior of fiber composite materials with a ductile matrix, whose tensile strength is larger than of the fibers itself (according to Fig. 1.12) is shown. Above the critical fiber content $\Phi_{F,crit}$ the behavior is affected considerably by the fiber. On reaching the fiber strength a simple brittle failure develops and the composite material fails.

For composite materials with a brittle matrix, where no hardening arises and where the elongation to fracture is smaller than those of the fibers, the material fails on reaching the strength of the matrix below the critical fiber content (see Fig. 1.14). Above this critical parameter a higher number of fibers can carry more load and a larger reinforcement effect develops. In the case of a composite material with a ductile matrix and ductile fibers; where both exhibit hardening during the tensile test, the deformation behavior is, in principle, different (Fig. 1.15). The resulting

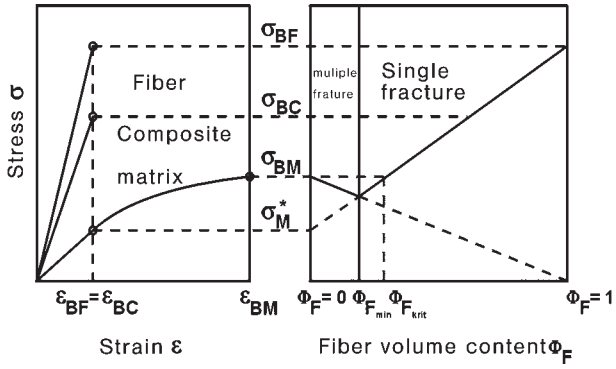

Fig. 1.14 Stress–strain behavior of a fiber composite material with a brittle matrix, which shows no strengthening behavior and whose elongation at fracture is smaller than that of the fibers (σ_{BF} = tensile strength of the fiber, σ^*_F = effective fiber strength at fracture of the composite material, σ_{BC} = strength of the composite material, σ_{BM} = matrix strength, ε_{BF} = elongation at fracture of the fiber, ε_{BM} = elongation at fracture of the matrix, ε_{BC} = elongation at fracture of composite material) [24].

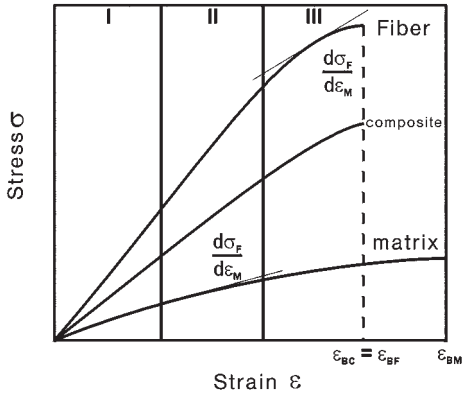

Fig. 1.15 Stress–strain behavior of fiber composite materials with a ductile matrix and fibers, both have strength in the tensile test (ε_{BF} = elongation at fracture of the fiber, ε_{BM} = elongation at fracture of the matrix, ε_{BC} = elongation at fracture of the composite material) [24].

stress–strain curve can be divided into three ranges: range I is characterized by the elastic behavior of both components by a Young's modulus in accord with the linear mixture rule. In range II only the matrix shows a strain hardening, the fiber is still elastically elongated. Here the composite material behaves as represented in Fig. 1.13. In range III both matrix and fiber show strain hardening behavior: the composite material fails after reaching the fiber strength.

1.3.2 Short Fiber Reinforcement

The effect of short fibers as reinforcement in metallic matrixes can be clarified with the help of a micromechanical model (shear lay model). The influence of the fiber length and the fiber orientation on the expected strength can be shown as a function of the fiber content and the fiber and matrix characteristics with the help of simple model calculations. The starting point is the mixture rule for the calculation of the strength of an ideal long-fiber-reinforced composite material with load in the fiber direction (Eq. (1) [23]). For short-fiber reinforcement the fiber length has to be considered [25]. During the loading of the composite materials, e.g. by tensions, the individual short fibers do not carry the full tension over their entire length. Only with over tension and predominantly shear stresses at the fiber/matrix interface will the load transfer partly to the fiber. Figure 1.16 shows the modeling of the load of a single fiber, which is embedded in a ductile matrix and stressed in the fiber direction.

The effective tension on the fiber in dependence on the fiber length can be calculated as follows:

$$\frac{d\sigma_F}{dx} \cdot dx \cdot r_F{}^2 \cdot \pi + 2\pi \cdot \tau_{FM}\, r_F\, dx = 0 \tag{5}$$

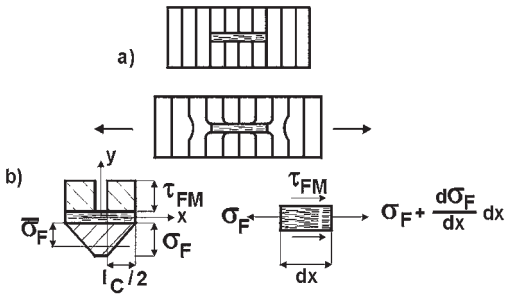

a) Strain field in the matrix
b) Shear strength at the interface fiber/matrix and tensile strength within the fiber

Fig. 1.16 Model of loading of a single fiber, embedded in a ductile matrix (after [23]): (a) Stress field in the matrix, (b) shear stress distribution at the interface fiber/matrix and tensile strength contribution in the fiber.

$$\sigma_F = \frac{2}{r_F} \cdot \tau_{FM} \cdot \left[\frac{2}{r_F} - x \right] \tag{6}$$

$$l_C = \frac{\sigma_F \cdot d_F}{2\,\tau_{FM}} \tag{7}$$

Where σ_F = fiber tension, r_F = fiber radius, d_F = fiber diameter, τ_{FM} = shear stress at the fiber/matrix interface. A critical fiber length l_C results, at which the fiber can be loaded to its maximum (Fig. 1.17).

The shear strength at the interface matrix/fiber is

$$\tau_{FM} = 0.5 \cdot \sigma_M^* \tag{8}$$

where σ_M^* = matrix yield point.

The effective fiber strength $\sigma_{F,eff}$ in dependence on the fiber length is

$$\sigma_{F,eff} = \eta \cdot \sigma_F \cdot \left(1 - \frac{l_c}{2 \cdot l_m} \right) \tag{9}$$

where η= fiber efficiency (deviation from optimum $0<\eta<1$) [28]; l_m= average fiber length.

According to Fig. 1.17 three cases, depending on the fiber length, can be distinguished [23–27]:

Fiber length $l_m > l_c$:

$$\sigma_C = \eta \cdot C \cdot \Phi_F \cdot \sigma_F \cdot \left(1 - d_F \cdot \frac{\sigma_F}{2 \cdot l_m \cdot \sigma_m^*} \right) \tag{10}$$

where C = orientation factor [26] (orientated $C = 1$, irregular $C = 1/5$, planar isotropic $C = 3/8$).

Fiber length $l_m = l_c$:

$$\sigma_C = \eta \cdot C \cdot 0.5 \cdot \Phi_F \cdot \sigma_F + (1 - \Phi_F) \cdot \sigma_M^* \tag{11}$$

Fiber length $l_m < l_c$:

$$\sigma_C = \eta \cdot C \cdot \sigma_M^* \cdot \frac{l_m}{2 \cdot d_F} + (1 - \Phi_F) \cdot \sigma_M^* \tag{12}$$

At a fiber length below the critical fiber length l_c the tensile strength of the fiber under load cannot be completely utilized. The reinforcement effect is lower [27]:

$$l_c = d_F \frac{\sigma_F - \sigma_M^*}{\sigma_M^*} \tag{13}$$

The models are based on idealised conditions: ideal adhesion between fiber and matrix and ideal adjustment and distribution of the long fibers or the arranged short fibers. Figure 1.18 shows schematically the influence of the length/thickness relationship of the fibers on the reinforcement effect under optimal conditions. By

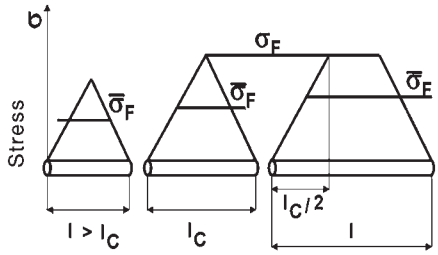

Fig. 1.17 Dependence of the effective fiber strength on the fiber length ($\sigma_F = \sigma_{F,eff}$), after [24].

increasing the fiber length the potential of long fibers (l/d 100) will be approached. For irregular or planar-isotropically arranged short fibers an optimal distribution is the basic condition for applicability. The result of an estimation is shown in Fig. 1.19. It represents the relationship of the strength of fiber-reinforced light metal alloys, calculated with Eqs. (1) and (10)–(12), to the strength of the non-reinforced matrix (reinforcement effect) as a function of the content of aligned fibers for different fiber length [29]. For the matrix characteristics the following mechanical properties at room temperature were used: tensile strength, 340 MPa; yield strength, 260 MPa. The aluminum oxide fiber Saffil (fiber tensile strength, 2000 MPa; diameter, 3 µm) was the fiber used. At small fiber contents a reduction in strength first occurs, up to a minimum fiber volume content, above this value the strength increases until a fiber content ϕ_1–ϕ_4 (depending on the fiber length) is reached, this is the strength of the nonreinforced matrix. Thereafter the reinforcement effect increases with increasing fiber content and length.

The presented calculations presuppose an orientation of the fibers in the stress direction, with an irregular arrangement there is a smaller reinforcement effect.

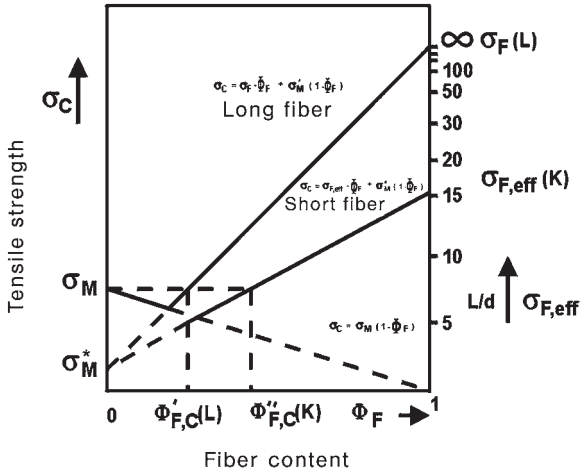

Fig. 1.18 Linear mixture rule of the tensile strength of unidirectional fiber composite materials, the right ordinate represents the effective fiber strength according to Eq. (9), after [23] and [27].

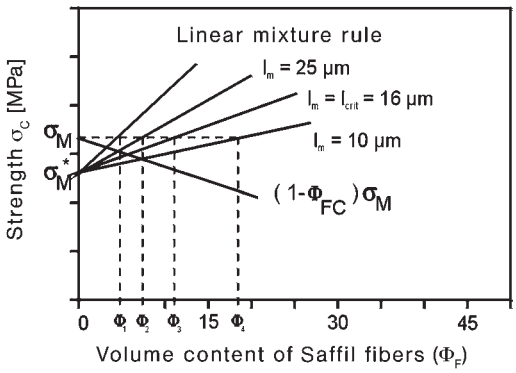

Fig. 1.19 Influence of the fiber length and volume content on the properties of magnesium composite materials (AZ91+Saffil-fibers) [28].

Figure 1.20 illustrates this using as an example magnesium alloy AZ91 strengthened by Saffil fibers. With increasing isotropy more fibers must be added in order to obtain a reinforcement effect. The amount of fibers required for the reinforcement effect is: for long fibers, a fiber content $\Phi_1 = 3.2$ vol%; for aligned short fibers Φ_2=3.5 vol% and for planar-isotropically distributed fibers Φ_3= 12.5 vol%. This effect increases with increasing load temperature, as shown in Fig. 1.21. This figure gives the calculated strength of composite materials for two different yield

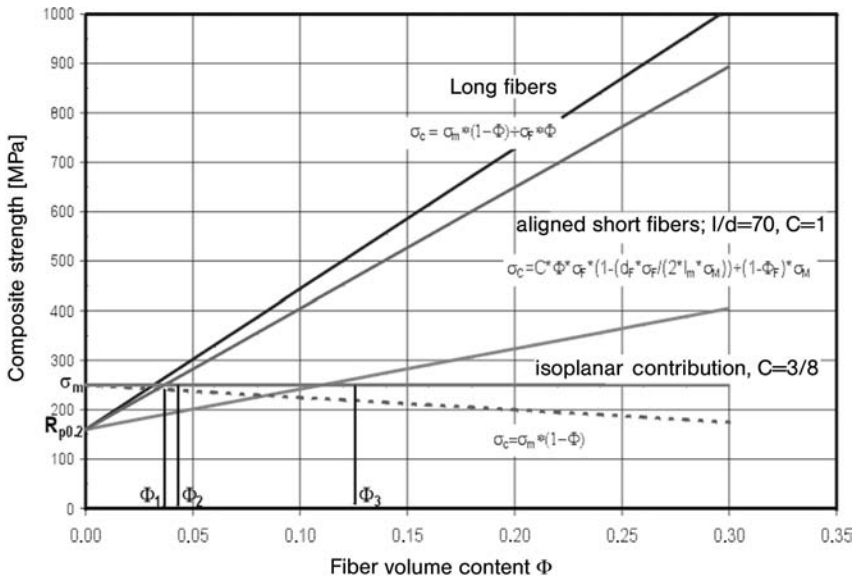

Fig. 1.20 Influence of the fiber length and fiber orientation on the composite material strength for the system magnesium alloy AZ91 (yield strength: 160 MPa, tensile strength 255 MPa) + C fiber (fiber strength 2500 MPa, fiber diameter 7 µm), schematic after Eqs. (1) and (10).

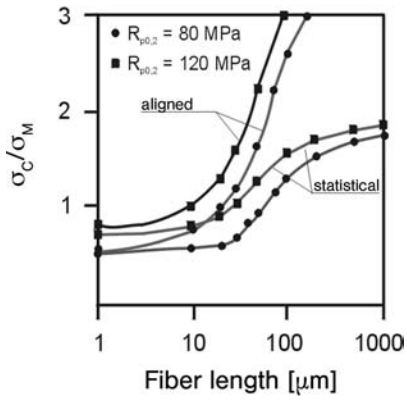

Fig. 1.21 Influence of the fiber length and fiber orientation on the reinforcement effect σ_C/σ_M for a composite material with 20 vol.% aluminum oxide fibers for different matrix yield strengths [29].

strengths of the nonreinforced matrix (80 MPa and 115 MPa) [29]. Although for the calculations only models with simplified boundary conditions were used, they show the objective for the production and processing of such composite materials. A goal is an optimal alignment of the fibers with the retention of a long fiber length.

1.3.3 Strengthening by Particles

The influence of ceramic particles on the strength properties of particle reinforced light metals can be described by using the following micromechanical model [30, 31]:

$$\Delta R_{p,C} = \Delta\sigma_\alpha + \sigma_{KG} + \Delta\sigma_{SKG} + \Delta\sigma_{KF} \tag{14}$$

where $\Delta R_{p,C}$ is the increase in tensile strength of aluminum materials by particle addition.

The influence of induced dislocations $\Delta\sigma_\alpha$ is given by:

$$\Delta\sigma_\alpha = \alpha \cdot G \cdot b \cdot \rho^{1/2} \tag{15}$$

with

$$\rho = 12\,\Delta T \frac{\Delta C \Phi_p}{bd} \tag{16}$$

where $\Delta\sigma_\alpha$ is the yield strength contribution due to geometrical necessary dislocations and inner tension, α is a constant (values 0.5–1), G is the shear modulus, b the Burger's vector, ρ the dislocation density, ΔT the temperature difference, ΔC the difference in thermal expansion coefficient between matrix and particle, Φ_p the particle volume content and d the particle size.

The influence of the grain size $\Delta\sigma_{KG}$ is given by:

$$\Delta\sigma_{KG} = k_{Y1}\, D^{-1/2} \tag{17}$$

with

$$D = d\left(\frac{1-\Phi_p}{\Phi_p}\right)^{1/3} \tag{18}$$

where $\Delta\sigma_{KG}$ is the yield strength contribution from changes in grain size (for example recrystallization during thermomechanical treatment of composite materials, analogue Hall-Petch); k_{Y1} is a constant, D is the resulting grain size and Φ_p is the particle volume content.

The influence of the grain size $\Delta\sigma_{SKG}$ is given by:

$$\Delta\sigma_{SKG} = k_{Y2} \cdot D_s^{-1/2} \tag{19}$$

with

$$D_s = d\left(\frac{\pi d^2}{6\Phi_p}\right)^{1/2} \tag{20}$$

where $\Delta\sigma_{SKG}$ is the yield strength contribution due to changes in subgrain size (for example in a relaxation process during thermomechanical treatment of composite materials), k_{Y2} is a constant (typical value 0.05 MN m$^{-3/2}$), D_s is the resulting subgrain size and Φ_p is the particle volume content.

The yield point is usually measured as the yield strength with 0.2 % remaining elongation. A significant strain hardening occurs, which is dependent on the particle diameter and content.

The strain hardening contribution $\Delta\sigma_{KF}$ is given by

$$\Delta\sigma_{KF} = KG\,\Phi_p\left(\frac{2b}{d}\right)^{1/2} \cdot \varepsilon^{1/2} \tag{21}$$

where K is a constant, G the shear modulus, Φ_p the particle volume content, b the Burger's vector, d the particle diameter and ε the elongation.

According to whether the particle size or the particle content is the dominant effect, different characteristic tension contributions of the individual mechanisms to the technical yield strength $R_{P0.2}$ of the particle strengthened light metal alloys result. The example of a particle-strengthened composite material with two different particle diameters in Fig. 1.22 clarifies this in principle. Generally higher hardening contributions are made by smaller particle diameters than by coarser particles. For smaller particle diameters the work hardening and the grain size influence contributes the most to the increase in the yield strength. Figure 1.23 shows schematically the change in the substantial hardening contributions with increasing particle content for a constant particle diameter.

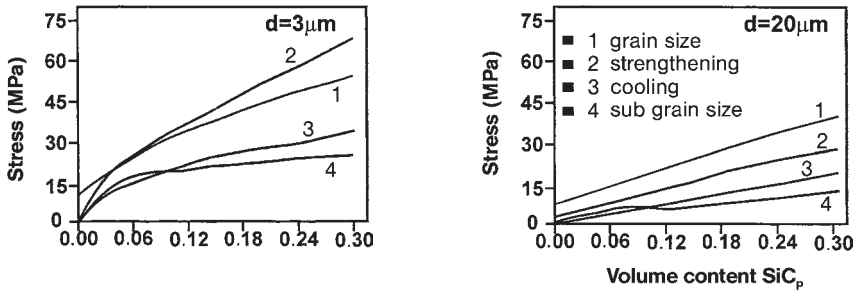

Fig. 1.22 Strain contribution of different mechanisms to the technical yield point calculated after the micromechanical model for aluminum alloys with SiC_P-addition, after [31].

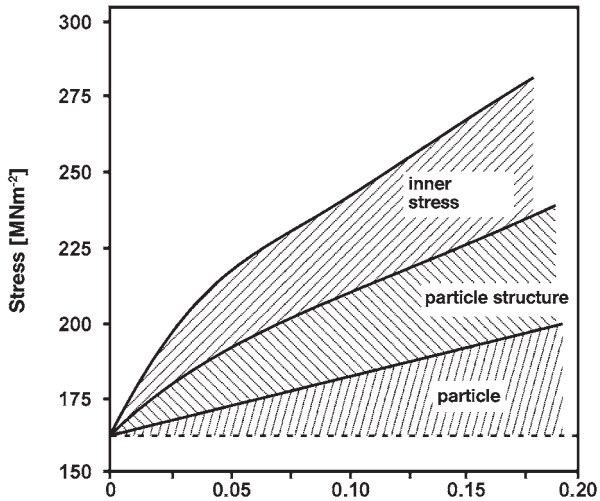

Fig. 1.23 Composition of particle reinforcement of various strengthening contributions (after [27]).

1.3.4 Young's Modulus

An objective in the development of light metal composite materials is to increase the modulus of elasticity (Young's modulus). Which potential arises here, can be estimated by the mixture rule, whereby the well-known border cases apply only to certain geometrical alignments of the components in the composite material. The universally used models are the following linear and inverse mixture rules [3]:

Linear mixture rule: Voigt-model (ROM)

$$E_C = \Phi_p E_p + (1 - \Phi_p) E_M \tag{22}$$

Inverse mixture rule: Reuss-model (IMR)

$$E_c = \left(\frac{\Phi_P}{E_P} + \frac{1 - \Phi_P}{E_M} \right)^{-1} \tag{23}$$

Where Φ_P is the volume content of particles or fibers, E_c the Young's modulus of the composite material, E_p the Young's modulus of the particle or fiber and E_M the Young's modulus of the matrix.

The Voigt model is only applicable for long-fiber-reinforced composite materials with a stress direction parallel to the fiber orientation, while the Reuss model applies to layer composite materials with a load perpendicular to the layers. An advancement of these models, which is also applicable for short fibers or particles, is the model by Tsai Halpin. By implementing an effective geometry factor, which can be determined from the structure of the composite materials as a function of the load direction, the geometry and the orientation of the reinforcement can be considered [32]:

$$E_c = \frac{E_M (1 + 2Sq\,\Phi_P)}{1 - q\,\Phi_P} \tag{24}$$

with:

$$q = \frac{(E_P/E_M) - 1}{(E_P/E_M) + 2S} \tag{25}$$

where S is the geometry factor of the fiber or particle ($1/d$).

Figure 1.24 presents as an example the Young's moduli calculated using Eqs. (22)–(25) for SiC particle reinforced magnesium materials as a function of the particle content and for different geometry factors according to Eqs. (24) and (25).

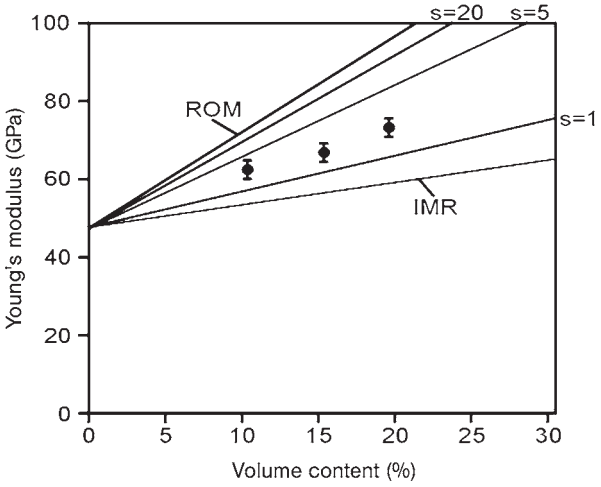

Fig. 1.24 Comparison of theoretically calculated Young's modulus values with the experimentally determined values for particle reinforced composite materials (ROM: linear mixture rule, IMR: inverse mixture rule [33].

Comparison of the measured Young's moduli is shown. A good agreement between calculated and experimental values can be seen; using a geometry factor $S=2$ for the applied SiC particles [33]. The basic condition for the application of such models is the presence of a composite material with an optimal structure, i.e. without pores, agglomerates of particles or nonreinforced areas.

1.3.5 Thermal Expansion Coefficient

Reinforcement of light metal alloys with ceramic fibers or particles entails a reduction in the thermal expansion coefficients. For this physical characteristic also, simple models are available to estimate the thermal expansion coefficients with the help of the characteristics of the individual components. The model of Schapery [34] was developed, in order to describe the influences on the thermal expansion coefficients:

$$\alpha_{3C} = \frac{E_F \alpha_F \Phi_F + E_M \alpha_M (1 - \Phi_F)}{E_C} \tag{26}$$

where α_{3C} is the axial thermal expansion coefficient, α_F the thermal expansion coefficient of the fibers and α_M the thermal expansion coefficient of the matrix.

$$\alpha_{1C} = (1 + \nu_M)\,\alpha_M \Phi_M + (1 + \nu_F)\,\alpha_F \Phi_F - \alpha_{3C}\,\nu_{31C} \tag{27}$$

$$\nu_{31C} = \nu_F \Phi_F + \nu_M (1 - \Phi_F) \tag{28}$$

where α_{1C} is the transverse thermal expansion coefficient, ν_F Poisson's ratio of the fibers and ν_M Poisson's ratio of the matrix.

Since the Schapery model is conceived for the calculation of thermal expansion coefficients for aligned long fibers the model can only be used for short-fiber reinforced materials with restrictions. A basic condition is an alignment of the short fibers. The thermal prehistory of the materials, in order to be able to proceed from a uniform internal tensile state, also has to be considered. A representation of calculated and measured values for the thermal expansion coefficients of light metal alloy composite materials for the example of a magnesium alloy reinforced with aligned Al_2O_3-short fibers (Saffil) is shown in Fig. 1.25. Here the upper curve represents the calculated values for the transverse thermal expansion coefficients and the lower curve the calculated values for the axial coefficient. The lower limit curve was calculated with the help of the theoretical Young's modulus according to the linear mixture rule of Eq. (22). When using the experimentally determined values of the Young's modulus of the composite material, then the values marked by squares result. In this case the deviations from the optimal structure are considered to be in good agreement, for the Mg+15 vol% Al_2O_3, with the measured axial expansion coefficients. This agreement with the real measured Young's modulus of the composite materials can be found also when using particles as reinforcement [35].

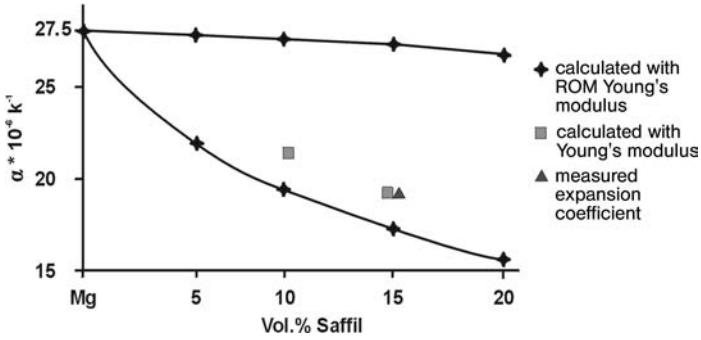

Fig. 1.25 Change in the thermal expansion coefficient with increasing fiber content (model after Shapery [34]) [33].

The thermal expansion coefficient is determined by the thermal prehistory of the composite materials, which results from the production and the application. Essentially the internal strain exercises influence. Figure 1.26 shows the temperature dependence of the thermal expansion coefficients of the monolithic magnesium alloy QE22 and the composite material QE22 + 20 vol % Saffil fibers for different orientations of the fibers. With the monolithic materials the expansion coefficient increases with increasing temperature. The same applies to the composite material with a fibers oriented perpendicular to the level of the planar-isotropic distribution of the fibers (90°). Since the fibers there are not optimally effective a lower reduction in the expansion develops. With increasing temperature the difference between the reinforced and the nonreinforced matrixes becomes less. In the case of an orientation parallel to the fiber level (0°) a stronger reduction effect results,

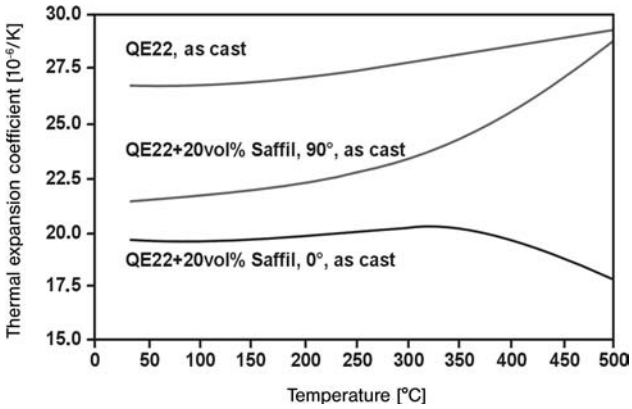

Fig. 1.26 Dependence of the thermal expansion coefficient of magnesium composite materials on the temperature and fiber orientation in comparison to the nonreinforced matrix [36].

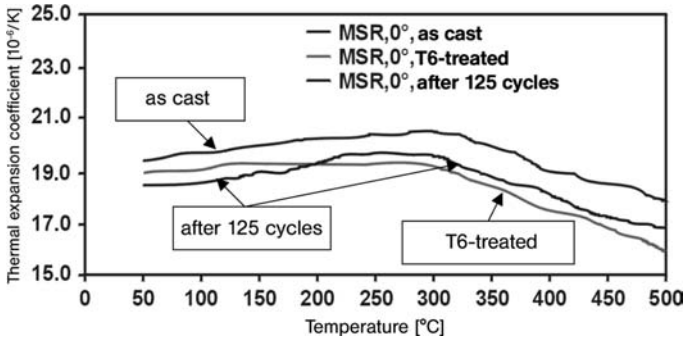

Fig. 1.27 Influence of the thermal prehistory on the expansion behavior of aluminum oxide fiber reinforced magnesium composite materials [36].

which increases with increasing temperature. The influence of the thermal prehistory on the thermal expansion coefficients is represented in Fig. 1.27 for the example of the magnesium alloy MSR + vol % Saffil. For the cast condition a comparable process results, as shown in Fig. 1.24. After a T6-heat treatment the curve shifts to higher values, particularly in the temperature range above the ageing temperature (204°C). After a thermal cyclic load a reduction in the internal strain appears and results in further increase in the values.

1.4 Interface Influence

Compared with monolithic materials the microstructure and the interfaces of metal matrix composite materials cannot be considered in isolation, they are mutually related. Chemical interactions and reactions between the matrix and the reinforcement component determine the interface adhesion, modify the characteristics of the composite components and affect the mechanical characteristics significantly.

In high temperature use of MMCs the microstructure has to remain stable for long service periods. Thermal stability and failure is determined by changes in the microstructure and at the interfaces, e.g. reaction and precipitation processes. Thermal stress of MMCs can take place both isothermally and cyclically. The effects show differences. During a cyclic load of monolithic materials, especially at high temperature gradients and cycle speeds, a high probability of failure by thermal fatigue is to be expected, e.g. short-fiber reinforced aluminum alloys possess good thermal shock stability.

The formation of the interface between the matrix and the reinforcing phase has a substantial influence on the production and characteristics of the metallic composite materials. The adhesion between both phases is usually determined by the interaction between them. During the production of the molten matrix e.g. by infiltration, wettability becomes significant.

1.4.1 Basics of Wettability and Infiltration

Basically the wettability of reinforcement with a metal melt can be shown by the edge angle adjustment of a molten droplet on a solid base as the degree of wettability according to Young:

$$\gamma_{SA} - \gamma_{LS} = \gamma_{LA} \cdot \cos \Theta \tag{29}$$

where γ_{LA} is the surface energy of the liquid phase, γ_{SA} the surface energy of the solid phase, γ_{LS} the interface energy between the liquid and solid phases and Θ is the edge angle.

Figure 1.28 shows the edge angle adjustment of a molten droplet on a solid base for different values of the interface energy. At an angle of $>\pi/2$ a nonwettable system is described and for an angle limit of $<\pi/2$ a wettable system. With decreasing angle the wettability improves. In Table 1.3 the surface and interface stresses of selected metal – ceramic systems at different temperatures are summarized. Of special relevance is the system Al/SiC, since it is the basis for the melting metallurgy of particle reinforced aluminum composite materials.

As the contact develops, for example at the beginning of an infiltration, adhesion occurs. The adhesion work W_A for separation is [41]:

$$W_A = \gamma_{SA} - \gamma_{LA} = \gamma_{LS} \tag{30}$$

$$W_A = \gamma_{LA} \cdot (1 + \cos \Theta) \tag{31}$$

Tab. 1.3 Surface and interface strains of selected metal–ceramic systems at different temperatures.

Alloy, Ceramic, Systems	*Temperature (K)*	γ_{la} *(mJ m^{-2})*	γ_{lsa} *(mJ m^{-2})*	γ_{ls} *(mJ m^{-2})*	*Ref.*
Al	953	1050	–	–	37
Mg	943	560	–	–	37
Al_2O_3	0	–	930	–	38
MgO	0	–	1150	–	38
Cu/Al_2O_3	1370	1308	1485	2541	39
	1450	1292	1422	2284	39
Ni/Al_2O_3	1843	1751	1114	2204	39
	2003	1676	988	1598	39
Al/SiC	973	851	2469	2949	40
	1073	840	2414	2773	40
	1173	830	2350	2684	40

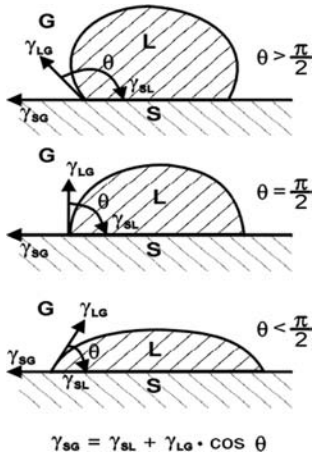

Fig. 1.28 Edge angle adjustment of a melt drop on a solid base for various values of the interface energy (after Young).

In the case of immersion the interface between the solid and the atmosphere disappears, while the interface between the solid and the liquid forms. The immersing work W_I is:

$$W_I = \gamma_{LS} - \gamma_{SA} \tag{32}$$

In the case of spreading the liquid is spread out on a solid surface. During this procedure the solid surface is reduced as well as a new liquid surface being formed and hence a new solid/liquid interface is formed. The spreading work W_S is:

$$W_S = \gamma_{SA} - \gamma_{LS} - \gamma_{LA} \tag{33}$$

The wetting procedure is kinetic and is dependent on time and temperature. Therefore, the kinetics can be affected by the temperature. Figure 1.29 shows, as

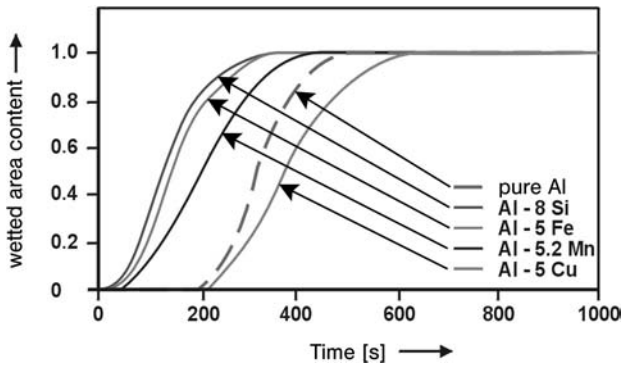

Fig. 1.29 Time dependence of the wetting degree (unit fraction) of SiC plates by aluminum melts at different alloy additions [42].

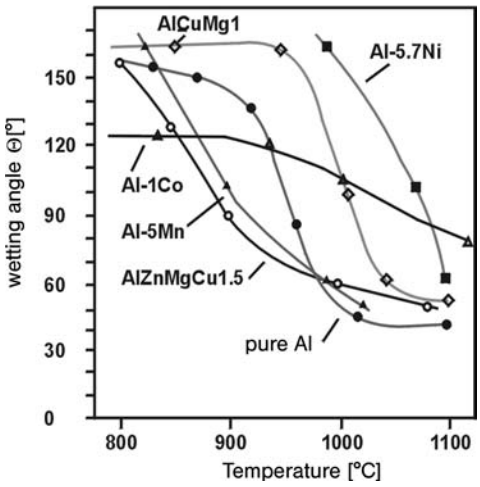

Fig. 1.30 Temperature dependence of the wetting angle of aluminum drops on a SiC plate [43].

an example of the time dependence of a wetting procedure, the wetting degree (surface fraction) of SiC plates by aluminum alloy melts of different composition. In Fig. 1.30 the temperature dependence of the wetting angle of one aluminum alloy droplet on a SiC plate is represented. Both figures show the further possibility of the influence of variation of the composition in the appropriate material system. The alloying elements act by changing the surface tension of the melt or by reaction with the reinforcement. On the one hand the composition of the matrix, or rather reinforcement, is modifiable and on the other hand there exists the possibility of purposeful influence by applying coatings on the intensifying phase. The role of a reaction at the interface is important, because from it a new system can result and the interface energies can be changed substantially, thus altering the wetting angle.

In Eq. (29) the change induced by the reaction, for example, of an oxide reinforcement Me_1O with a matrix alloy part Me_2, has to be taken into consideration [44]:

$$\gamma_{LS} - \gamma_{SA} = (\gamma_{LS} - \gamma_{SA})_0 - \Delta\gamma_r - \Delta G_r \tag{34}$$

$$Me_2 + Me_1O \leftrightarrow Me_2O + Me_1 \tag{35}$$

$$\gamma_{LA} \cdot \cos\Theta = (\gamma_{SA} - \gamma_{LS})_0 - \Delta\gamma_r - \Delta G_r \tag{36}$$

where $(\gamma_{ls} - \gamma_{sa})_0$ is the wettability without reaction, $\Delta\gamma_r$ the interface tension from the reaction of newly formed interfaces and ΔG_r the given free energy at the triple line solid/liquid/atmosphere (reaction energy).

Figure 1.31 shows the influence of pressure-free infiltration through different reactions by using different reactive binder systems and fiber contents such as Mg/Al_2O_3 fibers. With a very reactive SiO_2-containing binder premature infiltration happens at lower temperatures than with an Al_2O_3 binder [17].

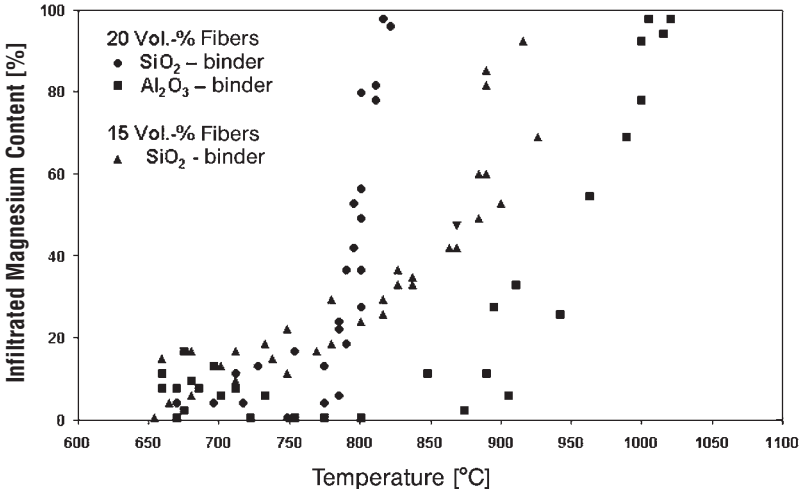

Fig. 1.31 Influence of pressure free infiltration by different reactions under use of different reactive fiber contents on the example of pure Mg/Al_2O_3 fibers, Dissertation Fritze and [17].

An additional possible influence exists through the change in the surrounding atmosphere or rather the atmosphere in the preform. It is possible, for example, that a preform before infiltration is flushed with gas, which can lead to a change in the oxygen partial pressure. Figure 1.32 shows the dependence of the wetting angle in the system Al_2O_3/pure aluminum on the temperature for two oxygen partial pressures [40]. For high partial pressures of oxygen high wetting angles occur at low temperatures. Only when starting from temperatures above 1150 K does the value for the wetting angle decrease to that for a low oxygen partial pressure. However, technically this influence is not relevant, because the atmosphere can be changed only with difficulty. An exception is the infiltration by the production of a vacuum (gas pressure infiltration); in this case gas pressures can be modified.

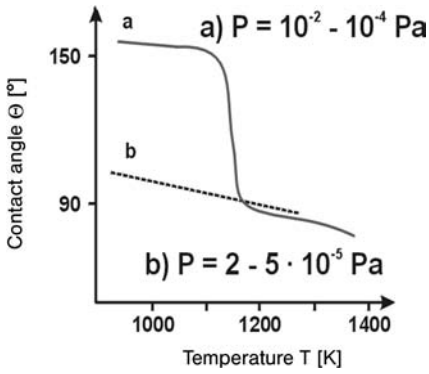

Fig. 1.32 Schematic presentation of the change in the wetting angle with change in the oxygen particle pressure [44].

Wetting for the actual infiltration procedure is of substantial importance. This is shown in a simple schematic representation in Fig. 1.33. In the case of good wetting (small edge angle) a capillary effect occurs (Fig. 1.33a). At large edge angles this procedure is inhibited (Fig. 1.33b). Additionally this can occur in technical processes by a reaction between the melt and the surrounding atmosphere. Then, for example, an oxide film forms, as in the case of magnesium alloys, which affects the wetting behavior by formation of a new interface between the reinforcement and the melt, as clarified in Fig. 1.34. The statements made above apply only to considerations close to the equilibrium. The influence of the wetting on the infiltration during technically relevant processes is thus less, if applied pressure on the melt, or rather the flow rate of the melt in the perform, determines the kinetics of the wetting, for example in the production of a wetted system by high pressure in the melt. However, the wetting nevertheless still has an influence on the adhesion of the components in the composite, which will later be described in more detail.

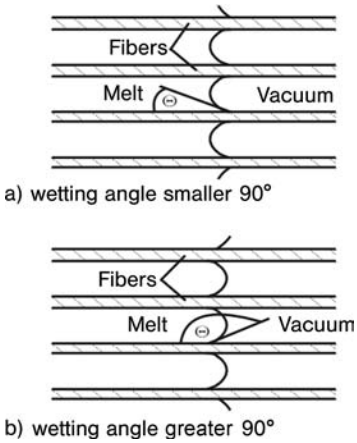

Fig. 1.33 Schematic presentation of an ideal melt infiltration of fiber preforms [45].

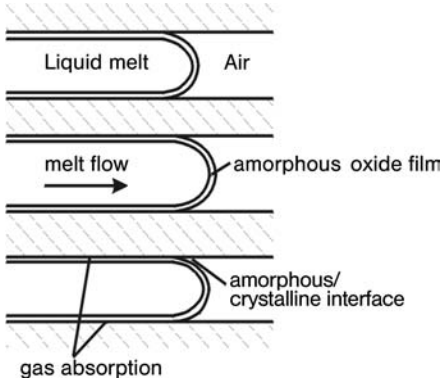

Fig. 1.34 Schematic presentation of the infiltration process of an aluminum oxide preform with molten aluminum [45].

The actual infiltration process for the production of metallic composite materials consists of several indexing steps: the formation of a contact between the melt and the reinforcement at the surface of a fiber or particle preform, the infiltration with the melt flow through the preform and the solidification procedure. At the beginning of the infiltration a minimum pressure must usually be developed, so that infiltration can follow. Usually a pressure-free spontaneous infiltration is not the rule, and is only possible with thin preforms with reactive systems and with long process times. The resulting pressure as driving force for the infiltration [46] is

$$\Delta P = P_0 - P_a - \Delta P_\gamma \tag{37}$$

where ΔP is the resulting pressure, the driving force for the reaction, $P_0$the pressure in the melt on entering the preform (see Fig. 1.35), P_a the pressure in the melt at the infiltration front (see Fig. 1.36), $\Delta P_\gamma$the pressure decrease in the melt at the infiltration front due to surface influences (effect of wettability).

When $P_0 = P_a$ a minimum infiltration pressure ΔP_μ can be defined:

$$\Delta P_\mu = \Delta P_\gamma = S_f(\gamma_{LS} - \gamma_{SA}) \tag{38}$$

where S_f is the surface interface per unit area.

Without external applied pressure the effect of induced infiltration by the capillary force can be presented as following [47]:

$$P_\gamma = \frac{2\,\gamma_{LA} \cdot \cos \Phi}{r} \tag{39}$$

where r is the radius of the capillary.

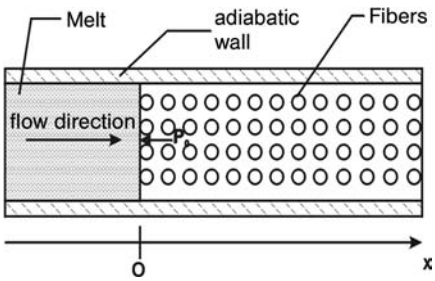

Fig. 1.35 Schematic presentation of an adiabatic, unidirectional infiltration, starting condition [46].

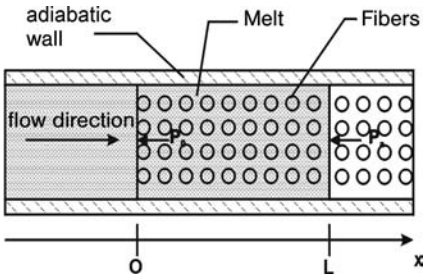

Fig. 1.36 Schematic presentation of an adiabatic, unidirectional infiltration [46].

Using the hydrostatic pressure

$$S_f = \frac{6\,V_f}{d_f\,(1 - V_f)} \tag{40}$$

results in the rising height:

$$h_S = \frac{2\,\gamma_{LA} \cdot \cos \Phi}{\rho \cdot g \cdot h} \tag{41}$$

where h_s is the rising height, g the gravitational constant and ρ the density.

As a pressure-free infiltration a preform consisting of many capillaries can be imagined and thus the influence of wettability and structure parameter (surface and pores – or rather capillary diameter) can be seen when introducing the following structure parameter in Eq. (38) [47]:

For a spherical particle:

$$S_f = \frac{6\,V_f}{d_f\,(1 - V_f)} \tag{42}$$

For a long fiber bunch and short fiber preform:

$$S_f = \frac{4\,V_f}{d_f\,(1 - V_f)} \tag{43}$$

Where V_f is the fiber or particle content and d_f is the fiber or particle diameter.

Table 1.4 shows the change in the specific surface with increasing fiber portion in the Al_2O_3-preform of Saffil fibers [48]. The specific surface also influences the permeability of a preform. This characteristic is important for the even supply of the preform with the melt and affects the necessary pressure for the infiltration. This is shown in Fig. 1.37 for Saffil preforms with water infiltration [48, 49]. It is noticeable that from fiber contents of 20 vol% the permeability is significantly reduced. In this context the viscosity of a melt also has an important influence. By variation of the temperature and composition optimisation of the infiltration process is controllable. Fig. 1.38 gives information on the change in the viscosity of magnesium and aluminum melts as a function of the temperature for unalloyed systems.

The previous considerations provide only an explanation of the processes and influencing variables on the wetting and infiltration, which are relevant in material systems, for example for stirring particles into melts or infiltrating. For both processes further procedures are of course relevant. Examples are the solidification

Tab. 1.4 Specific surface of Al_2O_3 preforms, after [17] and [48].

Fiber volume content of Al_2O_3 preforms [vol. %]	10	20	24	25
Specific surface: $S_f = 10^6$ fiber surfaces (m^2)/ pore volume (m^3)	1.26	3.41	4.39	4.58

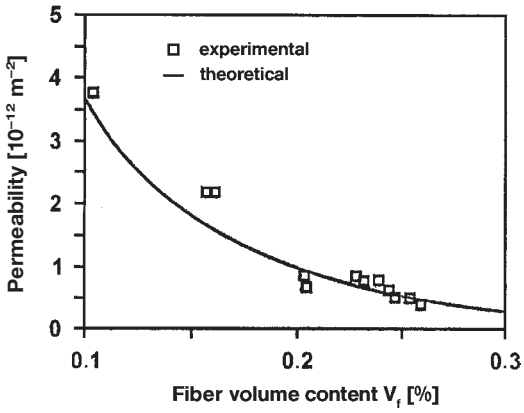

Fig. 1.37 Comparison of permeability of preforms for running water, after Mortensen and calculations of Sangini and Acrivos [48, 49].

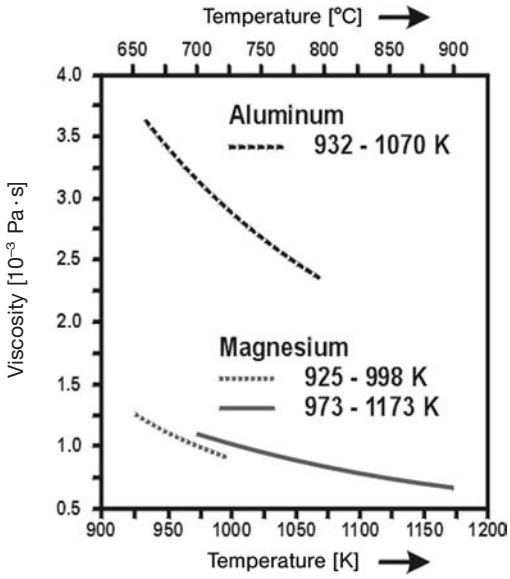

Fig. 1.38 Temperature dependence of the viscosity of magnesium and aluminum melts [50].

procedures of the melts. They overlay with the abovementioned procedures. For poor wetting of particles, for example in the production of particle-strengthened light alloys, a segregation or liquidization of the particles can take place. During the infiltration, solidification procedures can affect the permeability and prevent the complete treatment of the preform. Equation (38) (see Fig. 1.35 and 1.36) assumes a constant heat balance and no partial solidification. In reality there is heat dissipation over the tool and thus directed solidification occurs. Also the given free solidification heat has a substantial influence. The solidification worsens the permeability and influences the flow conditions in the preform. In reality a feed and a solidification procedure take place during the infiltration as a result of the directed heat

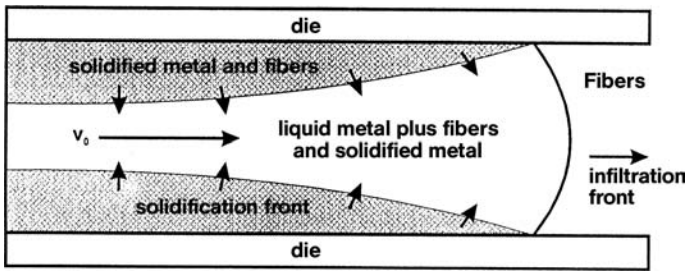

Fig. 1.39 Schematic presentation of solidification with external heat loss during a unidirectional infiltration [47].

dissipation, as represented in Fig. 1.39. The heat dissipation in the system preform/liquid or solidified melt is essentially determined by the thermal characteristics of the components (specific heat, thermal conductivity). Thus the reinforcements possess essentially higher specific heat values and smaller heat conductivities (exceptions are carbon fibers). In Table 1.5 these characteristic values are summarized for C and Al_2O_3 fibers. In the case of the applied alloys it is to be noticed that magnesium melts possess a smaller heat capacity than aluminum and therefore are processed at higher temperatures or the preforms have to be at higher temperatures than with aluminum alloys.

Tab. 1.5 Comparison of physical data of C fibers and aluminum oxide fibers (Saffil).

Fiber	*Specific heat* ($J\ m^{-3}\ K^{-1}$)	*Coefficient of thermal conductivity* ($W\ m^{-1}\ K^{-1}$)
Carbon P100	1.988×10^6	520
Carbon T300	1.124×10^6	20.1
Saffil	$2.31\ \times10^6$	0

1.4.2 Objective of Adhesion

The interaction between wetting and adhesion has already been briefly mentioned in Section 1.1. Figure 1.40 describes this connection using the example of the adhesive strength of a solidified aluminum melt dropped onto a substrate as a function of the wetting angle, determined by the droplet shear test. For small edge angles high adhesive strength values with a failure by shearing result. At larger angles the adhesive strength decreases and the failure only occurs under tension. In systems with good wettability reactions play a substantial role. The adhesion in composite systems can be improved by reaction. However, in some cases the reactions can become too distinctive, so that they result in damage to the reinforcement, e.g. reduction of the tensile strength of fibers. Thus the reinforcement po-

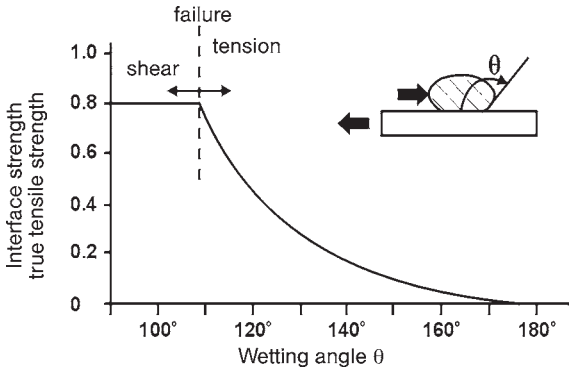

Fig. 1.40 Edge angle dependence of the adhesion strength of solidified Al melt drops [51].

tential is reduced. Later, brittle reaction products or pores can develop, which can again decrease the adhesion. Fot the example of the system Ni and Al_2O_3 in Fig. 1.41 it is clear that an optimum must be sought. With a proceeding reaction bonding is improved and the fiber strength decreases. In the case of poor binding the interface fails and the fiber failure dominates with increasing binding. In Fig. 1.42 the formation of an interface between an Al_2O_3 fiber and a magnesium alloy is represented for two conditions. In the cast condition in Fig. 1.42b only sporadic discontinuous MgO particles occur. The fibers are negligibly damaged and possess their full reinforcement effect. After a long-term annealing treatment the reaction products have grown and the fibers are damaged, the strength of the composite material decreases (see Fig. 42a) [53]. In an example of a thermal treatment of the composite material system magnesium alloy AZ91/Al_2O_3 fiber/(Saffil) the connection between reaction layer thickness and strength properties can be clarified. An untreated composite material of this system has a tensile strength of 220 MPa [54].

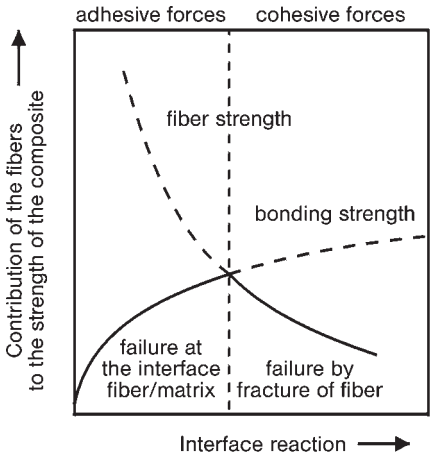

Fig. 1.41 Dependence on the reaction layer thickness of the shear strength of the interface between Ni and Al_2O_3 [52].

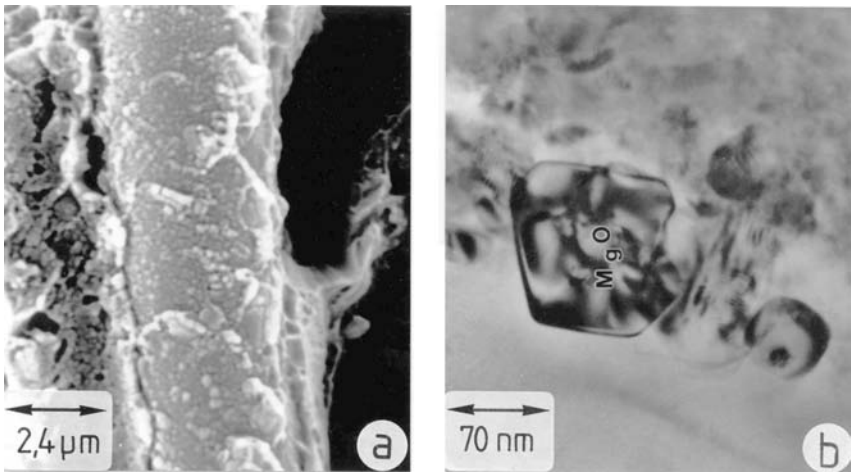

Fig. 1.42 Reaction products at the interface Mg alloy/Al_2O_3 fiber [53]:
(a) SEM image, long term loading 350 °C, 250 h; (b)TEM image, as-cast condition.

With increasing reaction layer thickness the tensile strength decreases to more than 50 % of the output strength (Fig. 1.43). With support of thermodynamic calculations the risk of this damage can be estimated. Also the influence of the reaction by layer systems on fibers [2, 22] or by modification of the alloy composition [55] is calculable and thus predictable.

The formation of the interface has, as discussed, a crucial influence on the behavior of the metallic composite materials. The influence of the elastic constants and the mechanical properties on the failure is substantial. As an example the change in the crack growth behavior in fiber composite materials is represented schematically in Fig. 1.44. In the case of weak binding (Fig. 1.44a) the crack moves along the fiber, the interface delaminates and the stress leads to the fracture of the

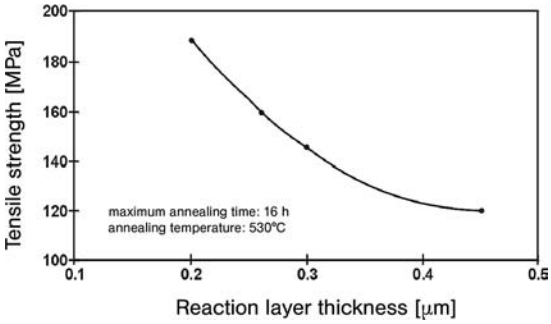

Fig. 1.43 Transverse pull strength of the fiber composite material AZ91/20 vol % Al_2O_3 fibers in dependence on the reaction layer thickness as a function of annealing time at 530 °C [54].

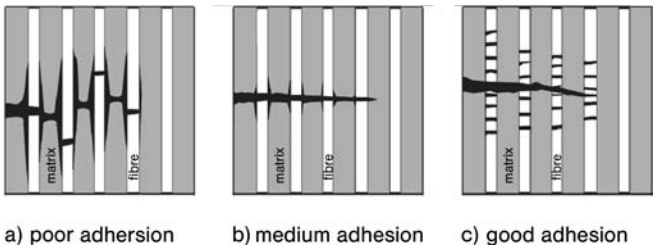

Fig. 1.44 Schematic presentation of the fiber/matrix dependence of the adhesion of a crack run [56, 57].

fibers successively. A classical "fiber pull out" develops. In the fracture image, for example the tensile test sample of a titanium composite material with SiC fibers (Fig. 1.45a) or aluminum alloy with C fibers (Fig. 1.46a), pulled out fibers are sporadically visible. For the case of very good adhesion of the matrix on the fiber no delamination (Fig. 1.44c) occurs. The crack opens up due to the tensile stress and the matrix deforms, due to the good adhesion the fiber is fully loaded and malfunctions. During further load the matrix continues to deform above the fiber fracture area also, thus the fiber is further loaded above and below the separation and malfunctions in further fragments. Macroscopically a brittle failure without pulling out of fibers (Fig. 1.45b, 1.46c,d) develops.

Depending on the interface formation transitions at very small delamination and fiber pull out also result (Fig. 1.44b and 1.46b). The adhesion for the tensile strength perpendicular to the fiber alignment (transverse pull strength) is of substantial importance, see Fig. 1.47 and 1.48. With very poor adhesion the fibers or particles work like pores and the strength is less than for the nonstrengthened matrix (Fig. 1.47a). In the case of very good binding a failure occurs in the matrix (Fig. 1.47c and 1.48a,b) or by disruption of the fiber (Fig. 1.47d and 1.48c). The strength of the composite material is comparable to the nonstrengthened matrix. At an average adhesion a mixed fracture occurs (Fig. 1.47b).

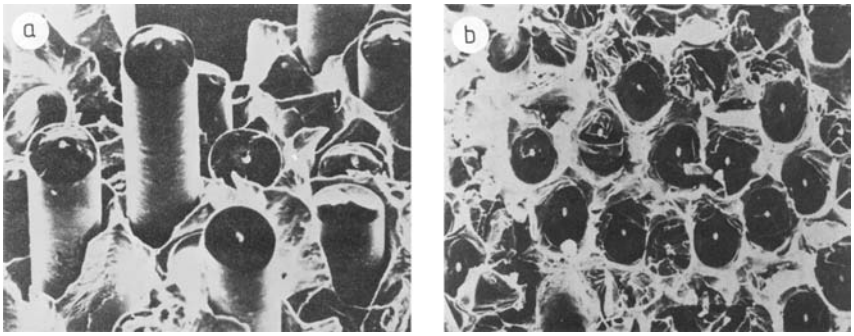

Fig. 1.45 Fracture surface in a monofilament composite material [58]:
(a)low interface shear strength; (b) high interface shear strength.

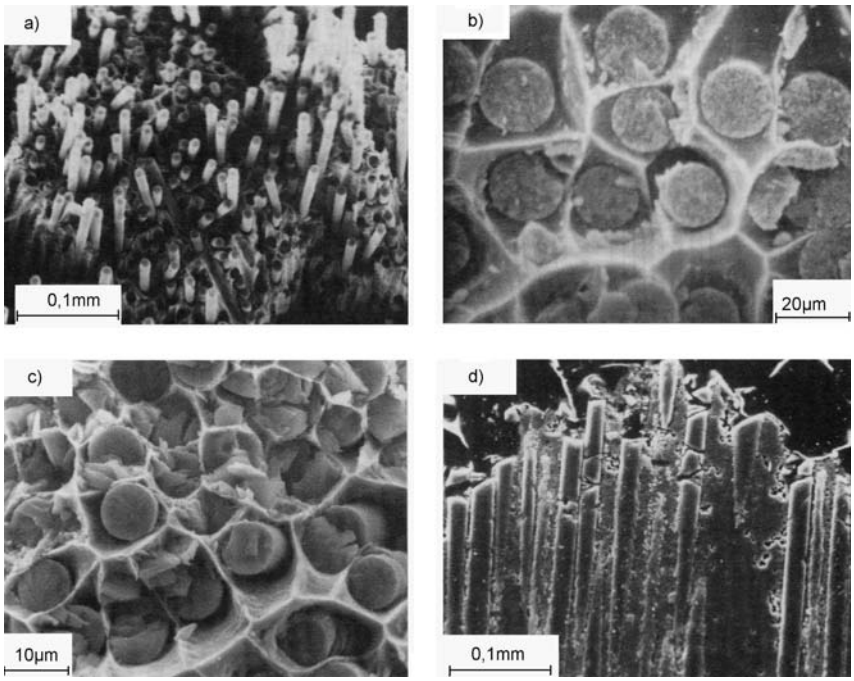

Fig. 1.46 Fracture surfaces in aluminum composite materials after tensile strain vertical to the fiber orientation [57]: (a) fiber/matrix- delamination (C/Al, weak adhesion); (b) shearing of fibers and dimple formation of a deformed matrix on the fibers (Al_2O_3/Al-2.5Li, medium adhesion); (c) Fracture in the matrix (SiC/Al good adhesion); (d) fracture run in multiple broken fibers (SiC/Al good adhesion).

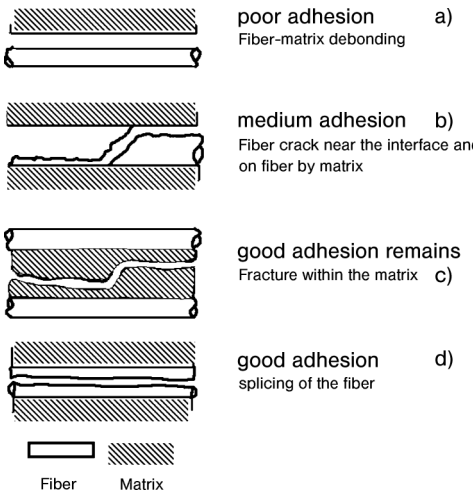

Fig. 1.47 Failure mechanism (schematic) in fiber composite materials for loading vertical to the fiber orientation [57].

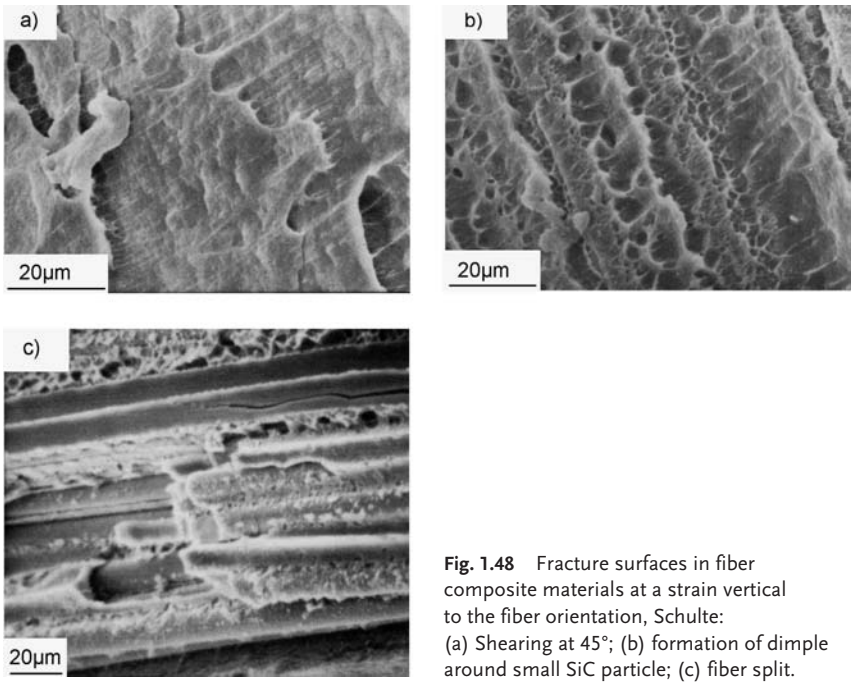

Fig. 1.48 Fracture surfaces in fiber composite materials at a strain vertical to the fiber orientation, Schulte: (a) Shearing at 45°; (b) formation of dimple around small SiC particle; (c) fiber split.

1.5 Structure and Properties of Light Metal Composite Materials

The structure of the composite materials is determined by the type and form of the reinforcement components, whose distribution and orientation are affected by the manufacturing processes. For composite materials, which are reinforced with long fibers, extreme differences result with different fibers. For multi-filament-strengthened composite materials (Fig. 1.49) the fiber/fiber contacts and nonreinforced areas are recognizable as a result of the infiltration of fiber bunch preforms. Structure defects, like fiber/fiber contacts, pores and nonreinforced areas are visible, which have a substantial influence on the composite characteristics. Figure 1.50 shows the optimal structure of a SiC monofilament/Ti composite material. With

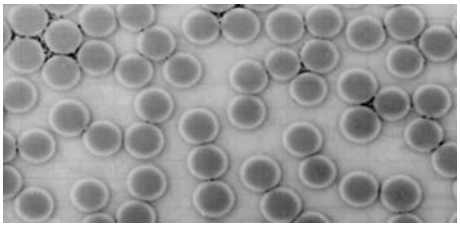

Fig. 1.49 Structure of a unidirectional endless fiber reinforced aluminum composite material (transverse grinding) [59]: matrix: AA 1085, 52 vol.% 15 µm Altex-fiber (Al_2O_3).

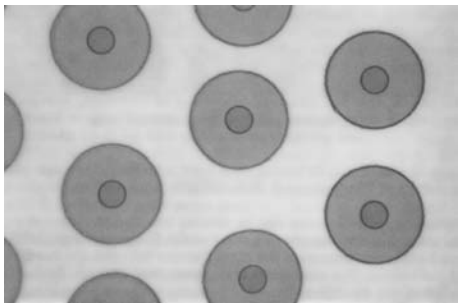

Fig. 1.50 Structure of a titan matrix composite material of SiC monofilaments [60].

monofilament-reinforced materials and with wire composite superconductors (Fig. 1.51 and 1.52) the uniformity of the fiber arrangement which result from the production process is remarkable. In Table 1.6 the material properties of different light alloy composite materials with continuous fibers are shown.

Figure 1.53 shows typical structure images of short-fiber reinforced light alloys. With short-fiber reinforced composite materials a planar-isotropic distribution of

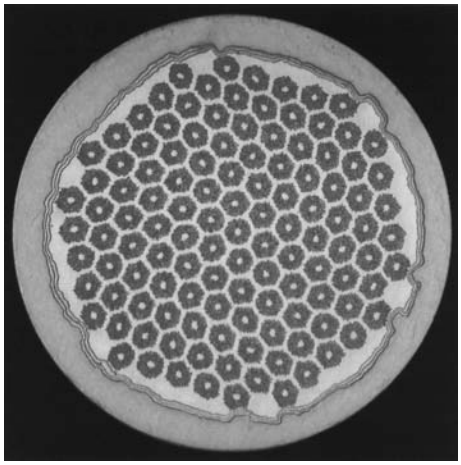

Fig. 1.51 Composite superconductor type Vacryflux NS 13 000 Ta: 13000 Nb filaments in CuSn and 35 % stabilization material 30 % Cu + 5 % Ta) in a shell [61].

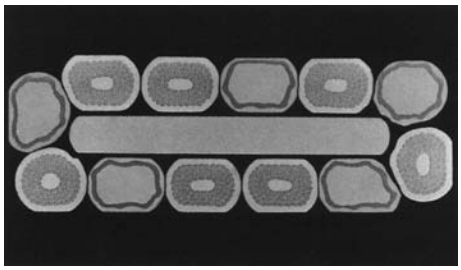

Fig. 1.52 Composite superconductor cable consisting of 7 superconductor cables and 5 stabilisation cables [61].

Tab. 1.6 Selected properties of typical long fiber reinforced light metal composites.

Material		*Fiber content (%)*	*Density (g cm^{-3})*	*Tensile strength (MPa)*	*Young's modulus (GPa)*	*Ref.*
System	***Orientation***					
Monofilaments						
B/Al	0°	50	2.65	1500	210	22
B/Al	90°	50	2.65	140	150	22
SiC/TiAl6V4	0°	35	3.86	1750	300	17, 5
SiC/TiAl6V4	90°	35	3.86	410		20, 2
Multifilaments						
SiC/Al	0°	50	2.84	259	310	21, 4
SiC/Al	90°	50	2.84	105		19, 3
Al_2O_3/Al–Li	0°	60	3.45	690	262	16, 9
Al_2O_3/Al–Li	90°	60	3.45	172–207	152	21, 4
C/Mg-Leg	0°	38	1.8	510		16, 6
C/Al	0°	30	2.45	690	160	6, 4
SiC/Al	Al + 55–70 % SiC		2.94		226	7, 2
MCX-736™	Al + 55–70 % SiC		2.96		225	7, 3

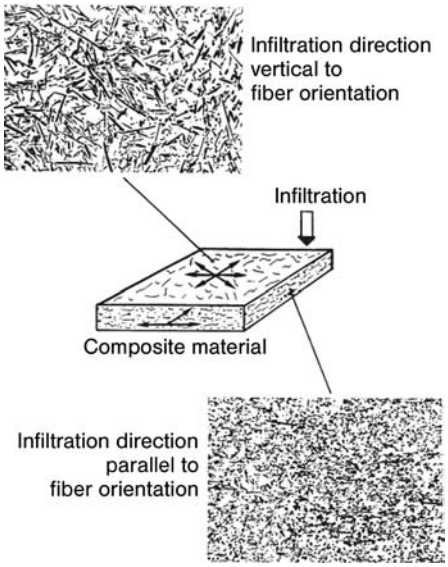

Fig. 1.53 Structure of formation of short fiber reinforced light metal composite materials [62].

the short fibers develops, due to the fiber molded padding production. The pressure-supported sedimentation technology leads to a layered structure. The infiltration direction is generally perpendicular to these layers. A reinforcement of light metal cast alloys by short fibers does not lead exclusively to an increase in strength, e.g. at room temperature, as the objective. It leads to a strength increase with increasing fiber content, as the example of AlSi12CuMgNi with a fiber content of 20 vol.% (Fig. 1.54) shows. However, the achievable effect is not economically justified in practice. The improvement in the properties, particularly at higher temperature where a doubling of the strength occurs (Fig. 1.54) and the strength properties under alternating flexural stress at 300°C (Fig. 1.55), makes the material interesting for applications such as pistons or for reinforced cylinder surfaces in engines. A dramatic increase in the temperature alternating resistance at the same application temperature is attainable, see Fig. 1.56.

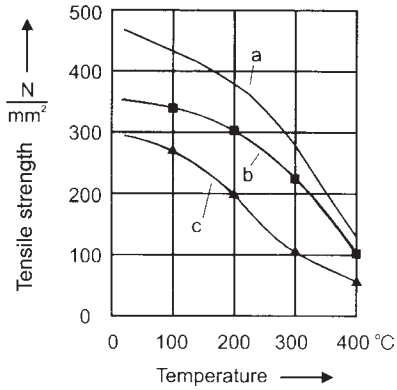

Fig. 1.54 Comparison of temperature dependence of the tensile strength of nonreinforced and reinforced piston alloy AlSi12CuMg (KS 1275) [13]: (a) KS 1275 with 20 vol.% SiC whisker; (b) KS 1275 with 20 vol.% Al_2O_3 fibers; (c) KS 1275 nonreinforced.

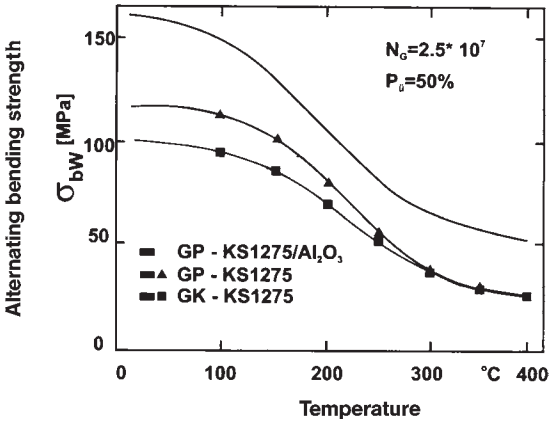

Fig. 1.55 Change in the alternating bending strength of nonreinforced and reinforced piston alloy (20 vol.% Al_2O_3 fibers) AlSi12CuMgNi (KS1275), with increasing temperature (GK = mold casting, GP = die casting) [14].

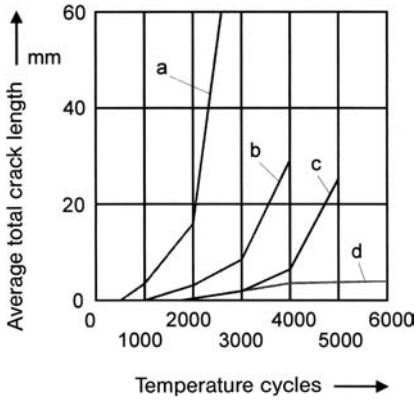

Fig. 1.56 Temperature shock resistance of the fiber reinforced piston alloy AlSi12CuMgNi (KS1275) for different fiber contents for a temperature of 350 °C [13]: (a) Nonreinforced, (b)12 vol.% Al_2O_3 short fibers, (c)17.5 vol.% Al_2O_3 short fibers, (c) 20 vol.% Al_2O_3 short fibers.

The cast particle-reinforced light alloys show typical particle distributions depending on the processing methods. Gravity die cast materials show nonreinforced areas due to the solidification conditions (Fig. 1.57a); while with pressure die cast materials the distribution of the particles is more optimal (Fig. 1.57b). Even better results are reached after the extrusion of feed material (Fig. 1.57c). In powder metallurgically manufactured composite materials (Fig. 1.57d) the extremely homogeneous distribution of the particles is noticeable after the extrusion

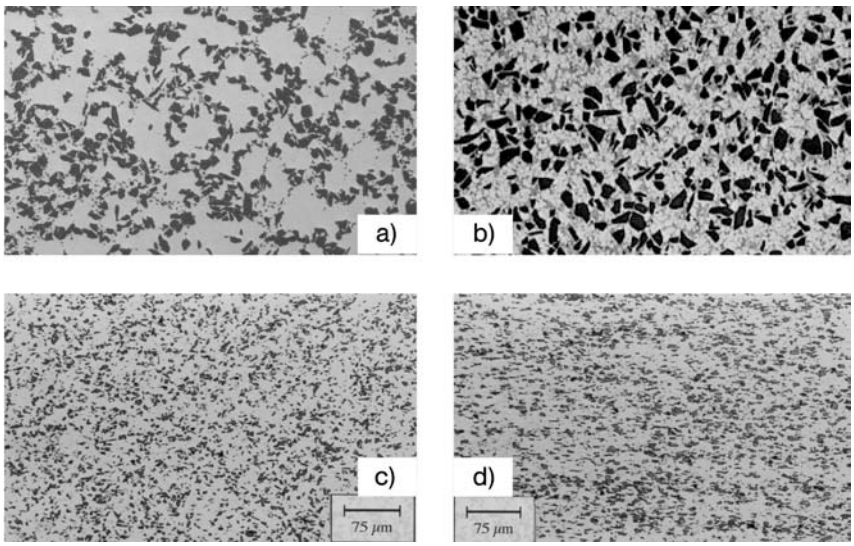

Fig. 1.57 Arrangement of typical structures of different particle reinforced light metal composite materials: (a) SiC-particle reinforced Al (mold cast [9]), (b) SiC-particle reinforced Al (die cast [10]), (c) SiC-particle reinforced Al (extruded powder mixture [11]), (d) SiC- particle reinforced Al (cast and extruded).

of powder mixtures. The possibility of combining particles and fibers to form a hybrid-reinforced composite material with the different effects of both reinforcement components is shown in Fig. 1.58.

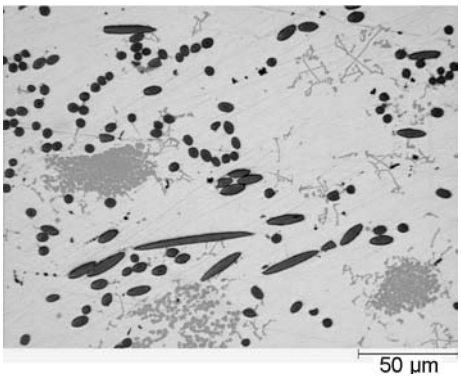

Fig. 1.58 Structure of formation of hybrid reinforced light metal composite materials with C short fibers and Mg_2Si particles [63].

With particle addition to light metals like aluminum, the hardness, the Young's modulus, the yield strength, the tensile strength and the wear resistance increase and the thermal expansion coefficient decreases. The order of magnitude of the improvement of these characteristics depends on the particle content and the selected manufacturing process. In Tables 1.7 and 1.8 characteristics of different particle-reinforced aluminum alloys are presented. In melting metallurgically manufactured materials by mixing in particles (Table 1.7) the upper limit of the particle addition is approx. 20 vol%. This limit is technically justified since a maximum tensile strength of over 500 MPa and a Young's modulus of 100 GPa are attainable with this particle content. Higher particle contents are made possible by reaction infiltration procedures, however, the materials then take on a more ceramic character becoming susceptible to brittle failure and, during tensile stress, a premature failure without plastic deformation takes place. However, the low thermal expansion despite the metallic character of these materials is outstanding.

For spray formed materials (Table 1.8) the limit for the particle content is approximately 13–15 vol%. However, the utilisation of special alloy systems, e.g. with lithium addition, can nevertheless lead to high specific characteristics. In powder metallurgical materials processed by extrusion from powder mixtures the particle content can be increased to over 40 vol%. Along with the fine-grained structure of the matrix, very high strength (up to 760 MPa), very high Young's modulus (up to 125 GPa) and low expansion coefficients (approximately 17×10^{-6} K^{-1}) are attainable. Unfortunately also the elongation at fracture and fracture toughness are worsened, however, the values are better than those of cast materials.

Tab. 1.7 Selected properties of typical aluminum cast composites, processed by ingot-, die cast or reaction infiltration, Manufacturers instruction after [11, 12, 16]. (T6 = solution annealed and artificially aged; T5 = artificially aged; *after ASTM G-77: Cast iron 0.066 mm^3; **CTE = thermal expansion coefficient, (a) after ASTM E-399 and B-645; (b) after ASTM E-23).

Material		*Yield stress (MPa)*	*Tensile strength (MPa)*	*Ultimate strain (%)*	*Young's modulus (GPa)*	*(a) Fracture toughness (b) Impact strength*	*Wear* Volume decrease (mm^3)*	*Thermal conductivity 22 °C ($cal\ cm^{-1}\ s^{-1}\ K^{-1}$)*	*CTE** 50–100 °C ($10^{-6}\ K^{-1}$)*
Name	***Composition***								
Gravity die casting (Chill casting)						(a) (MPa $m^{1/2}$)			
A356-T6	AlSi7g	200	276	6.0	75.2	17.4	0.18	0.360	21.4
F3S.10S-T6	AlSi9Mg10SiC	303	338	1.2	86.9	17.4			20.7
F3S.20S-T6	AlSi9Mg20SiC	338	359	0.4	98.6	15.9	0.02	0.442	17.5
F3K.10S-T6	AlSi10CuMgNi10SiC	359	372	0.3	87.6				20.2
F3K.20S-T6	AlSi10CuMgNi20SiC	372	372	0.0	101			0.346	17.8
Die casting						(b) (J)			
A390		241	283	3.5	71.0	1.4	0.18	0.360	21.4
F3D.10S-T5	AlSi10CuMnNi10SiC	331	372	1.2	93.8	1.4		0.296	19.3
F3D.20S-T5	AlSi10CuMnNi20SiC	400	400	0.0	113.8	0.7	0.018	0.344	16.9
F3N.10S-T5	AlSi10CuMnMg10SiC	317	352	0.5	91.0	1.4		0.384	21.4
F3N.20S-T5	AlSi10CuMnMg20SiC	338	365	0.3	108.2	0.7	0.018	0.401	16.6
Reaction infiltration		Flexural strength (MPa)		Density ($g\ cm^{-3}$)		(a) (MPa $m^{1/2}$)			
MCX-693™	Al+55-70% SiC	300	2.98	255	9.0		0.430	6.4	
MCX-724™	Al+55-70% SiC	350	2.94	226	9.4		0.394	7.2	
MCX-736™	Al+55-70% SiC	330	2.96	225	9.5		0.382	7.3	

Tab. 1.8 Properties of aluminum wrought alloy composites. Manufacturers instruction after [11, 12, 18–20].
(T6 = solution annealed and artificially aged; *after ASTM G-77: Cast iron 0.066 mm^3; **CTE = thermal expansion coefficient).

Material		*Yield stress (MPa)*	*Tensile strength (MPa)*	*Ultimate strain (%)*	*Young's modulus (GPa)*	*Fracture toughness (MPa $m^{1/2}$) ASTM E-399*	*Wear* volume decrease (mm^3)*	*Thermal conductivity 22°C (cal cm^{-1} s^{-1} K^{-1})*	*CTE** 50–100°C (10^{-6} K^{-1})*
Name	***Composition***								
Cast prematerial (extruded or forged)									
6061 -T6	AlMg1SiCu	355	375	13	75	30	10	0.408	23.4
6061 -T6	+ 10% Al_2O_3	335	385	7	83	24	0.04	0.384	20.9
6061 -T6	+ 15% Al_2O_3	340	385	5	88	22	0.02	0.336	19.8
6061 -T6	+ 20% Al_2O_3	365	405	3	95	21	0.015		
Powder metallurgically processed prematerial (extruded)									
6061 -T6	AlMg1SiCu	276	310	15	69.0				23.0
6061 -T6	+ 20% SiC	397	448	4.1	103.4				15.3
6061 -T6	+ 30% SiC	407	496	3.0	120.7				13.8
7090-T6		586	627	10.0	73.8				
7090-T6	+ 30% SiC	676	759	1.2	124.1				
6092-T6	AlMg1Cu1Si17.5SiC	448	510	8.0	103.0				
6092-T6	AlMg1Cu1Si25SiC	530	565	4.0	117.0				
Spray formed material (extruded)									
6061-T6	+ 15% Al_2O_3	317	359	5	87.6				
2618-T6	+ 13% SiC	333	450		89.0				19.0
8090-T6	AlCuMgLi	480	550		79.5				22.9
8090-T6	+ 12% SiC	486	529		100.1				19.3

1.6 Possible Applications of Metal Matrix Composites

Light alloy composite materials have, in automotive engineering, a high application potential in the engine area (oscillating construction units: valve train, piston rod, piston and piston pin; covers: cylinder head, crankshaft main bearing; engine block: part-strengthened cylinder blocks), see Table 1.9. An example of the successful use of aluminum composite materials within this range is the partially short-fiber reinforced aluminum alloy piston in Fig. 1.59, in which the recess range is strengthened by Al_2O_3 short fibers. Comparable construction unit characteristics are attainable only with the application of powder metallurgical aluminum alloys or when using heavy iron pistons. The reason for the application of composite materials is, as already described, the improved high temperature properties. Potential applications are in the area of undercarriages, e.g. transverse control arms and particle-strengthened brake disks, which can be also applied in the area of rail-mounted vehicles, e.g. for undergrounds and railway (ICE), see Fig. 1.60. In the

Tab. 1.9 Applications of metal composites.

I.	Drive shaft for people and light load motor vehicles (Fig. 1.61) [65]:	
	Material:	AlMg1SiCu + 20 vol. % Al_2O_3P
	Processing:	extrusion form cast feed material
	Development aims:	– high dynamic stability, high Young's modulus (95 GPa) – low density (2.95 g cm^{-3}) – high fatigue strength (120 MPa for $n = 5\times10^7$, $R = -1$, RT) – sufficient toughness (21.5 MPa $m^{1/2}$) – substitution of steels
II.	Vented passenger car brake disk (Fig. 1.62) [65]:	
	Material:	G-AlSi12Mg + 20 vol. % SiC_P
	Processing:	sand- or gravity die casting
	Development aims:	– high wear resistance (better than conventional cast iron brake discs) – low heat conductivity (factor 4 higher than cast iron) – substitution of iron materials
III.	Longitudinal bracing beam (Stringer) for planes (Fig. 1.63) [66]:	
	Material:	AlCu4Mg2Zr + 15 vol. % SiC_P
	Processing:	extrusion and forging of casted feed material
	Development aims:	– high dynamic stability. high Young's modulus (100 GPa) – low density (2.8 g cm^{-3}) – high strength (R_m = 540 MPa. $R_{P0.2}$ = 413 MPa. RT) – high fatigue strength (240 MPa for n = 5×10^7, $R = -1$, RT) – sufficient toughness (19.9 MPa $m^{1/2}$)
IV.	Disk brake calliper for passenger cars (Fig. 1.64) [67]:	
	Material:	Aluminium alloy with Nextel ceramic fibre 610
	Weight reduction:	55 % compared to cast iron.

Fig. 1.59 Partial short fiber reinforced light metal diesel pistons [13, 14].

following some potential construction units made out of aluminum matrix composite materials with data concerning materials, processing and development targets are presented.

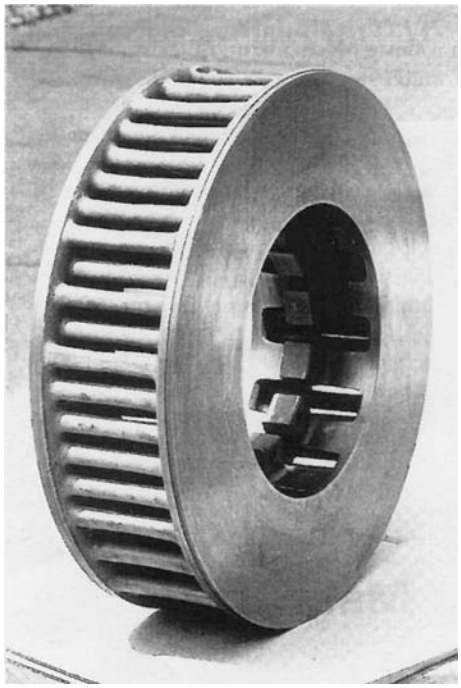

Fig. 1.60 Cast brake disk particle of reinforced aluminum for the ICE 2 [64].

Fig. 1.61 Drive shaft particle of reinforced aluminum for passenger cars of [65].

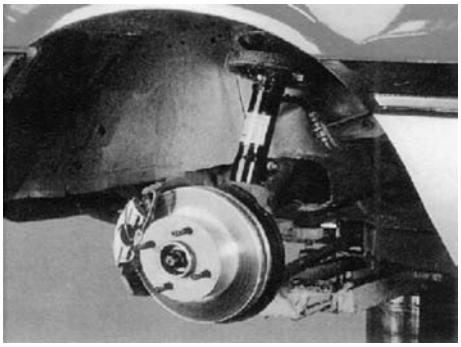

Fig. 1.62 Vented passenger car brake disk of particle reinforced aluminum [65].

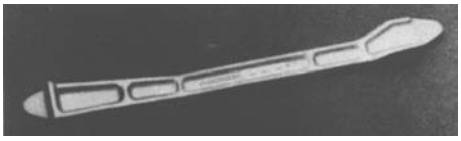

Fig. 1.63 Longitudinal bracing beam (Stringer) of particle reinforced aluminum [66].

Fig. 1.64 Disk brake calliper for passenger cars of conventional cast iron (left) and an aluminum matrix composite material (AMC) with Nextel® ceramic fiber 610 [67].

In the aviation industry the high specific strength, the high Young's modulus, the small thermal expansion coefficient, the temperature resistance and the high conductivity of the strengthened light alloys are of interest compared with polymer materials, e.g. for reinforcements, axle tubes, rotors, housing covers and structures for electronic devices. A compilation of potential and realized applications of most different metal matrix composites can be seen in Table 1.10.

Tab. 1.10 Potential and realistic technical applications of metal matrix composites.

Application	*Required properties*	*Material system*	*Processing technique*
Automotive and heavy goods vehicle			
Bracing systems, piston rods, frames, piston, piston pins, valve spring cap, brake discs, disc brake calliper, brake pads, cardan shaft	High specific strength and stiffness, temperature resistance, low thermal expansion coefficient, wear resistance, thermal conductivity	Al-SiC, Al-Al_2O_3, Mg-SiC, Mg-Al_2O_3, discontinuous reinforcements	Fusion infiltration, extrusion, forging, gravity die casting, die casting, squeeze-casting
Accumulator plate	High stiffness, creep resistance	PbC, Pb-Al_2O_3	Fusion infiltration
Military and civil air travel			
Axle tubes, reinforcements, blade- and gear box casing, fan and compressor blades	High specific strength and stiffness, temperature resistance, impact strength, fatigue resistance	Al-B, Al-SiC, Al-C, Ti-SiC, Al-Al_2O_3, Mg-Al_2O_3, Mg-C continuous and discontinuous reinforcements	Fusion infiltration, hot pressing, diffusion welding and soldering, extrusion, squeeze-casting
Turbine blades	High specific strength and stiffness, temperature resistance, impact strength, fatigue resistance	W super alloys, z. B. Ni_3Al, Ni-Ni_3Nb	Fusion infiltration, aligned solidification near net-shaped components
Aerospace industry			
Frames, reinforcements, aerials, joining elements	High specific strength and stiffness, temperature resistance, low thermal expansion coefficient, thermal conductivity	Al-SiC, Al-B, Mg-C, Al-C, Al-Al_2O_3, continuous and discontinuous reinforcements	Fusion infiltration, extrusion, diffusion welding and joining (spacial structures)
Energy techniques (electrical components and conducting materials)			
Carbon brushes	High electrical and thermal conductivity, wear resistance	Cu-C	Fusion infiltration, powder metallurgy
Electrical contacts	High electrical conductivity, temperature and corrosion resistance, burn-up resistance	Cu-C, Ag-Al_2O_3, Ag-C,Ag-SnO_2, Ag-Ni	Fusion infiltration, powder metallurgy, extrusion, pressing
Super conductor	Superconducting, mechanical strength, ductility	Cu-Nb, Cu-Nb_3Sn, Cu-YBaCO	Extrusion, powder metallurgy, coating technologies
Other applications			
Spot welding electrodes	Burn-up resistance	Cu-W	Powder metallurgy, infiltration
Bearings	Load carrying capacity, wear resistance	Pb-C, Brass-Teflon	Powder metallurgy, infiltration

1.7 Recycling

Of special economic and ecological interest for newly developed materials is the necessity for recirculation of arrears, cycle scrap and other material from these composites into the material cycle. Since ceramic materials usually occur in the form of particles, short fibers or continuous fibers for the reinforcement of metallic materials, a material separation of the components with the goal being the reuse of the matrix alloy and the reinforcement is almost impossible. However, with conventional melting treatments in remelting factories the matrix alloy can be recycled without problems.

In melting or powder metallurgically manufactured discontinuous short fiber or particle-strengthened light alloys reuse of the composite materials from cycle scrap or splinters can be possible under certain conditions. Particularly for particle-strengthened aluminum cast alloys the use of cycle scrap is possible, however splinters on direct remelting cause difficulties due contamination problems. Ref. [69] gives an overview of different recycling concepts for light alloy composite materials in relation to the alloy composition, the kind of reinforcement and the production and processing prehistory.

References

1 G. Ondracek, *Werkstoffkunde: Leitfaden für Studium und Praxis*, Expert-Verlag, Würzburg (**1994**).

2 *TechTrends*, International Reports on Advanced Technologies: Metal Matrix Composites: Technology and Industrial Application, Innovation 128, Paris (**1990**).

3 T. W. Clyne, P. J. Withers, *An Introduction to Metal Matrix Composites*, Cambridge University Press, Cambridge (**1993**).

4 K.U.Kainer, *Keramische Partikel, Fasern und Kurzfasern für eine Verstärkung von metallischen Werkstoffen. Metallische Verbundwerkstoffe*, K.U. Kainer (Ed.), DGM Informationsgesellschaft, Oberursel (**1994**), pp. 43–64.

5 H. Dieringa, K. U. Kainer, this report

6 K. U. Kainer, *Werkstoffkundliche und technologische Aspekte bei der Entwicklung verstärkter Aluminumlegierungen für den Einsatz in der Verkehrstechnik*, Newsletter TU Clausthal, Issue 82 (**1997**), pp. 36–44.

7 K. U. Kainer (Ed.), *Metallische Verbundwerkstoffe*, DGM Informationsgesellschaft, Oberursel (**1994**).

8 J. Schröder, K. U. Kainer, Magnesium Base Hybrid Composites Prepared by Liquid Infiltration, *Mater. Sci. Eng., A* **1991**, *135*, 33–36.

9 *DURALCAN Composites for Gravity Castings*, Duralcan USA, San Diego (**1992**).

10 *DURALCAN Composites for High-Pressure Die Castings*, Duralcan USA, San Diego (**1992**).

11 C. W. Brown, W.Harrigan, J. F. Dolowy, *Proc. Verbundwerk 90*, Demat, Frankfurt (**1990**), pp. 20.1–20.15.

12 *Manufacturers of Discontinuously Reinforced Aluminum (DRA)*, DWA Composite Specialities, Inc., Chatsworth USA (**1995**).

13 W.Henning, E. Köhler, *Maschinenmarkt* **1995**, *101*, 50–55.

14 S. Mielke, N. Seitz, Grosche, *Int. Conf. on Metal Matrix Composites*, The Institute of Metals, London (**1987**), pp. 4/1–4/3.

15 H. P. Degischer, Schmelzmetallurgische Herstellung von Metallmatrix-Verbundwerkstoffen, in *Metallische Verbundwerkstoffe*, K.U.Kainer (Ed.), DGM Informationsgesellschaft, Oberursel (**1994**), pp.139–168.

16 *Lanxide Electronic Components*, Lanxide Electronic Components, Inc., Newark USA (**1995**).

17 C. Fritze, Infiltration keramischer Faserformkörper mit Hilfe des Verfahrens des selbstgenerierenden Vakuums, Dissertation TU Clausthal (**1997**).

18 A. G. Leatham, A. Ogilvy, L. Elias, *Proc. Int. Conf. P/M in Aerospace, Defence and Demanding Applications*, MPIF, Princeton, USA (**1993**), pp. 165–175.

19 Cospray Ltd. Banbury, U.K., **1992**.

20 *Keramal Aluminum-Verbundwerkstoffe*, Aluminum Ranshofen Ges.m.b.H., Ranshofen, Österreich (**1992**).

21 F. Koopmann, Kontrolle Heft 1/2 (**1996**), pp. 40–44.

22 K. K. Chawla, *Composite Materials: Science and Engineering*, Springer-Verlag, New York (**1998**).

23 D. L. McDanels, R. W. Jech, J. W. Weeton, Analysis of Stress-Strain Behavior of Tungsten-Fiber-Reinforced Copper Composites, *Trans. Metall. Soc. AIME* **1965**, *223*, 636–642.

24 J. Schlichting, G. Elssner, K. M. Grünthaler, *Verbundwerkstoffe, Grundlagen und Anwendung*, Expert-Verlag, Renningen (**1978**).

25 A. Kelly, *Strong Solids*, Oxford University Press, London (**1973**).

26 C. M. Friend, The effect of matrix properties on reinforcement in short alumina fiber-aluminum metal matrix composites, *J. Mater. Sci.* **1987**, *22*, 3005–3010.

27 A. Kelly, G. J. Davies, The Principles of the Fiber Reinforcement of Metals, *Metall. Rev.* **1965**, *10*, 1–78.

28 G. Ibe, Grundlagen der Verstärkung von Metallmatrix-Verbundwerkstoffen, in *Metallische Verbundwerkstoffe*, K.U.Kainer (Ed.), DGM Informationsgesellschaft, Oberursel (**1994**), pp.1–41.

29 K. U. Kainer, Strangpressen von kurzfaserverstärkten Magnesium-Verbundwerkstoffen, *Umformtechnik* **1993**, *27*, 116–121.

30 F. J. Humphreys, Deformation and annealing mechanisms in discontinuously reinforced metal-matrix composites, *Proc. 9th Risø Int. Symp. on Mechanical and Physical Behavior of Metallic and Ceramic Composites*, S. I. Anderson, H. Lilholt, O. B. Pederson (Eds.), Risø National Laboratory, Roskilde (**1988**), pp. 51–74.

31 F. J. Humphreys, A. Basu, M. R. Djazeb, The microstructure and strength of particulate metal-matrix composites, *Proc. 12th Risø Int. Symp. on Materials Science, Metal-Matrix Composites – Processing, Microstructure and Properties*, N. Hansen et al. (Eds), Risø National Laboratory, Roskilde (**1991**), pp. 51–66.

32 J. C. Halpin, S. W. Tsai: Air Force Materials Laboratory (**1967**), AFML-TR-67-423.

33 F. Moll, K. U. Kainer, Properties of Particle Reinforced Magnesium Alloys in Correlation with Different Particle Shapes, *Proc. Int. Conf. Composite Materials 11*, Vol. III, pp. 511–519.

34 R. A. Schapery, *J. Comp. Mater.* **1968**, *23*, 380–404.

35 K. U. Kainer, U. Roos, B. L. Mordike, Platet-Reinforced Magnesium Alloys, *Proc. 1st Slovene-German Seminar on Joint Projects in Materials Science and Technology*, D. Kolar, D. Suvorov (Eds.), Forschungszentrum Jülich (**1995**), pp. 219–224.

36 C. Köhler, Thermische Beständigkeit von Kurzfaser-verstärkten Magnesium-Al_2O_3-Verbundwerkstoffen, Dissertation TU Clausthal (**1994**).

37 F. Delanny, L. Froyen , A.Deruyttiere, *J. Mater. Sci.* **1987**, *22*, 1–16.

38 J. Haag, *Bedeutung der Benetzung für die Herstellung von Verbundwerkstoffen unter Weltraumbedingungen – Größen, Einflüsse und Methoden-*, BMBF-Research Report W 81-021 (**1980**).

39 U. Angelopoulos, U. Jauch, P. Nikolopoulos, *Mat.-wiss. u. Werkstofftechnik* **1988**, *19*, 168–172.

40 S. Y. Oh, J. A. Cornie, K. C. Russel, Particulate Welding and Metal: Ceramic Interface Phenomena, Ceramic Engineering and Science, *Proc. 11th Annual Conf. On Composites and Advanced Materials* (**1987**).

41 K. C. Russel, S.Y. Oh , A. Figueredo, MRS Bull. **1991**, *16*, 46–52.

42 T. Choh, T. Oki, *Mater. Sci. Technol.* **1987**, *3*, 378.

43 R. Warren, C.-H. Andersson, *Composites* **1984**, *15*, 101.

44 A. Mortensen, I. Jin, *Int. Met. Rev.* **1992**, *37*, 101–128

45 G. A. Chadwick, *Mater. Sci. Eng., A* **1991**, *135*, 23–28.

46 A. Mortensen, L.J. Masur, J. A. Cornie, M. C. Flemings, *Metall. Trans. A* **1989**, *20*, 2535–2547.

47 A. Mortensen, J. A. Cornie, *Metall. Trans. A* **1987**, *18*, 1160–1163.

48 A. Mortensen, T. Wong , *Metall. Trans. A* **1990**, *21*, 2257–2263.

49 A.S. Sangini, A. Acrivos, *J. Multiphase Flow*, **1982**, *8*, 193–206.

50 R. P. Cchabra, D. K. Sheth, *Z. Metallkde.* **1990**, *81*, 264– 271.

51 L. J. Ebert, P. K. Wright: Mechanical Aspects of the Interface, in *Interfaces in Metal Matrix Composites*, A. G. Metcalfe (Ed.), Academic Press, New York (**1974**), p. 31.

52 R. F. Tressler, Interfaces in Oxide Reinforced Metals, in *Interfaces in Metal Matrix Composites*, A. G. Metcalfe (Ed.), Academic Press, New York (1974), p. 285.

53 K. U. Kainer, Herstellung und Eigenschaften von faserverstärkten Magnesiumverbundwerkstoffen, in: DGM Informationsgesellschaft, K. U. Kainer (Ed.), Oberursel (**1994**), pp. 219–244.

54 I. Gräf, K. U. Kainer, Einfluß der Wärmebehandlungen bei Al_2O_3-kurzfaserverstärktem Magnesium, *Prakt. Metall.* **1993**, *30*, 540–557.

55 K. U. Kainer, Alloying Effects on the Properties of Alumina-Magnesium-Composites, in *Metal Matrix Composites – Processing Microstructure and Properties*, N. Hansen et al. (Ed.), Risø National Laboratory, Roskilde (**1991**), pp. 429–434.

56 E. Fitzer, G. Jacobsen, G. Kempe in *Verbundwerkstoffe*, G. Ondracek (Ed.) DGM Oberursel (**1980**), p. 432.

57 Schulte in *Metal Matrix Composites – Processing Microstructure and Properties*, N. Hansen et al. (Ed.), Risø National Laboratory, Roskilde (**1991**), pp. 429–434.

58 J. M. Wolla, *Proc. Int. Conf. ISTFA 87: Advanced Materials*, Los Angeles (**1987**), p. 55

59 J. Janczak et al., *Grenzflächenuntersuchungen an endlosfaserverstärkten Aluminummatrix Verbundwerkstoffen für die Raumfahrttechnik*, Oberflächen Werkstoffe (**1995**) Heft 5.

60 http//www.mmc-asses.tuwien.ac.at/data/mfrm/tisic.htm#top3.

61 *Vaccumschmelze: Superconductors*, Corporate publications SL 021 (**1987**)

62 K. U. Kainer, B. L. Mordike, *Metall* **1990**, *44*, 438–443.

63 H. Dieringa, T. Benzler, K.U. Kainer, Microstructure, creep and dilatometric behavior of reinforced magnesium matrix composites, in *Proc. of ICCM13, Peking*, **2001**, p. 485.

64 F. Koopmann, *Kontrolle* Issue 1/2 (**1996**), pp. 40–44.

65 P. J. Uggowitzer, O. Beffort, Aluminumverbundwerkstoffe für den Einsatz in Transport und Verkehr. Ergebnisse der Werkstofforschung, Volume 6, M. O. Speidel, P. J. Uggowitzer (Eds.), Verlag "Thubal-Kain", ETH-Zürich (**1994**), 13–37.

66 C. Carre, V. Barbaux, J. Tschofen, *Proc. Int. Conf. on PM-Aerospace Materials*, MPR Publishing Services Ltd, London (**1991**), pp. 36-1–36-12.

67 3M Metal Matrix Composites, *Firmenschrift* 98-0000-0488-1(51.5)ii (**2001**).

68 K. U. Kainer, Konzepte zum Recycling von Metallmatrix-Verbundwerkstoffen, in *Recycling von Verbundwerkstoffen und Werkstoffverbunden*, G. Leonhardt, B. Wielage (Eds.), DGM Informationsgesellschaft, Frankfurt (**1997**), pp. 39–44.